EQUALIZATION TECHNIQUES FOR BROADBAND WIRELESS NETWORKS

by

Homa Eghbali

B.A.Sc., American University of Sharjah, Sharjah, U.A.E, 2009

Thesis submitted in partial fulfillment
of the requirements for the degree of

Masters of Science

In the School
of
Engineering Science

SIMON FRASER UNIVERSITY
Spring 2010

APPROVAL

Name: Homa Eghbali

Degree: Masters of Science

Title of Thesis: Equalization Techniques for Broadband Wireless Networks

Examining Committee: Dr. Jie Liang, Chair

Dr. Sami Muhaidat, Senior Supervisor

Dr. Rodney G. Vaughan, Supervisor

Dr. Paul K. M. Ho, Internal Examiner

Date Approved: April 6, 2010.

Declaration of
Partial Copyright Licence

Abstract

Wireless sensor networks (WSNs) are characterized by low-power devices equipped with communication capabilities. Due to the lack of a set infrastructure, WSNs exhibit characteristics fundamentally different from traditional networks. The existing literature in conventional wireless networks, therefore, cannot be applied to WSN design.

The recently introduced Cooperative diversity techniques exploit the broadcast nature of wireless transmission, creating a virtual antenna array through cooperating nodes. This form of diversity is therefore well suited for WSNs. The research in this field is however, still in it's infancy. Particularly, most of the current literature in this area assumes an idealized transmission environment with an underlying frequency-flat fading channel model and perfect channel state information, which are far away from being realistic if wideband sensor applications or mobile sensor networks are considered.

Motivated by these practical concerns, this thesis addresses the analysis and design of efficient equalization techniques for non-cooperative and cooperative wireless networks.

Dedication

To My Dearest Parents and My Lovely Brother

Acknowledgement

I wish to thank my loving parents. Without their endless love, knowledge, wisdom, and guidance, I would not have the goals I have to strive and reach my dreams. I am heartily thankful to my senior supervisor, Professor Sami Muhaidat, whose encouragement, guidance and support from the initial to the final level enabled me to develop an understanding of the subject. I would like to thank Professor Naofal Al-Dhahir from university of Texas at Dallas and Professor Murat Uysal from university of Waterloo for their helpful cooperation.

I would also like to thank Professor Rodney G. Vaughan for serving on my supervisory committee and Professor Paul K. M. Ho for serving as the internal examiner of my thesis. It is also my honor to thank the defense chair, Professor Jie Liang, for his time and efforts. Lastly, I offer my regards and blessings to all of those who supported me in any respect during the completion of the project. Special thanks go to the current and past members of our lab, Jinyun Ren, Maryam Dehghan, Sayed Alireza Banani, and Saad Mahboob to name but a few, for their help and lively discussions on research, and beyond.

Homa

Publications

1) H. Eghbali, S. Muhaidat, and N. Al-Dhahir, "A Novel Receiver Design for Single-Carrier Frequency Domain Equalization in Broadband Wireless Networks with Amplify-and-Forward Relaying," Accepted to IEEE Transactions on Wireless Communications, January 2010

2) H. Eghbali, S. Muhaidat, and N. Al-Dhahir, "A New Reduced Complexity Detection Scheme for Zero-Padded OFDM Transmissions," submitted to IEEE Transactions on Signal Processing as a Correspondence, February 2010

3) H. Eghbali, S. Muhaidat, and N. Al-Dhahir, "A Low Complexity two Stage MMSE-Based Receiver for Single-Carrier Frequency-Domain Equalization Transmissions over Frequency-Selective Channels," IEEE GLOBECOM'09, Honolulu, Hawaii, USA, November 2009.

4) H. Eghbali, and M. El-Tarhuni, "Multipath Detection for TH-PPM UWB Systems," ISSPIT2009, Ajman, U.A.E , December 2009.

5) H. Eghbali, S. Muhaidat, and N. Al-Dhahir, "A Novel Reduced Complexity MMSE-based Receiver for OFDM Broadband Wireless Networks," IEEE WCNC 2010, Sydney, Australia, April 2010.

6) H. Eghbali, S. Muhaidat, and N. Al-Dhahir, "A Novel Reduced Complexity Detection Scheme for Distributed Single-Carrier Frequency Domain Equalization," to be submitted to IEEE VTC 2010.

7) H. Eghbali, S. Muhaidat, and N. Al-Dhahir, "Performance Analysis of Distributed Space-Time Block Codes Using Frequency Domain Equalization Techniques Over Nakagami-n fading Channels," to be submitted to IEEE GLOBECOM'10.

8) H. Eghbali, S. Muhaidat, and N. Al-Dhahir, "A New Receiver Design for Single-Carrier Frequency-Domain Equalization in Broadband Cooperative Networks ," to be submitted to IEEE GLOBECOM'10.

Contents

List of Tables

List of Figures

Chapter 1

Introduction

1.1 Thesis Motivation

Recent advances in miniaturization and low-cost, low-power electronics have led to active research in large-scale networks of small, wireless, low-power sensors and actuators. Pervasive sensing that is freed from the burden of infrastructure will revolutionize the way we observe the world around us. Sensor networks already automatically warn us of invisible hazards, i.e. the contaminants in the air we breath or the water we drink, and far-away earthquakes soon to arrive. WSNs can open the eyes of a new generation of scientist to phenomena never before observable, paving the way to new eras of understanding in the natural sciences. These networks are characterized by small, low-power devices equipped with sensing and communication capabilities. With numerous applications and impact on several industries, WSNs are envisioned to be a key technology area for enormous growth in the near future. WSNs exhibit characteristics fundamentally different from traditional networks, due to the lack of a set infrastructure. Therefore, it's not possible to apply the existing rich literature in conventional wireless networks to WSN designs.

Cooperative diversity is a form of diversity well studied for WSNs, exploiting the broadcast nature of wireless transmissions by creating a virtual antenna array through cooperative nodes. Although cooperative diversity has recently gained much attention, research in this field is still in its infancy. The pioneering works in this area address mainly information-theoretic aspects, deriving fundamental performance bounds. However, practical implementation of cooperative diversity requires an in-depth investigation of several physical layer

issues such as channel estimation, equalization, and synchronization integrating the underlying cooperation protocols and relaying modes. Moreover, most of the current literature in the area of cooperative diversity assume an idealized transmission environment with an underlying frequency-flat fading channel model and perfect channel state information, which can be justified for fixed infrastructure narrowband WSNs, but are far away from being realistic for wideband sensor applications or mobile sensor networks.

Motivated by the practical concerns aforementioned, the main purpose of this thesis is to investigate and develop low-power consuming and efficient equalization techniques for non-distributed and distributed wireless networks.

1.2 Outline and Main Contributions

In chapter 2, we provide a brief review of important background materials related to the thesis. We first review different diversity techniques for fading channels including time diversity, frequency diversity, and space diversity, followed by an introduction to different diversity combining techniques. We then introduce the important concepts that will be used extensively throughout the thesis, including transmit diversity, space-time coding, cooperative diversity, multi-carrier modulation schemes, single carrier frequency-domain equalization (SC-FDE), orthogonal frequency division multiplexing (OFDM), and space-time block coded (STBC) SC-FDE.

In chapter 3, we study a new detection scheme for zero-padding (ZP)-OFDM. Recently, ZP-OFDM has been proposed as an alternative solution to coded-OFDM, which often incurs high decoding complexity. Various ZP-OFDM receivers have been proposed in the literature, trading off performance with complexity. To trade-off Bit Error Rate (BER) performance for extra savings in complexity, two low complexity equalizers for ZP-OFDM are derived in [1]. However, the BER performance of the two sub-optimal receivers proposed in [1] is not as good as minimum mean square error (MMSE)-ZP-OFDM. We propose a novel reduced complexity receiver design for ZP-OFDM transmissions, that not only outperforms MMSE-ZP-OFDM, but also uses low-complexity computational methods that bring a significant power saving to the proposed receiver. This makes it a strong candidate for WSNs which are characterized by small and low-power devices. We show that linear processing collects both multipath and spatial diversity gains, leading to significant improvement in performance, while maintaining low complexity. The material of this chapter has appeared in [2].

In chapter 4, we introduce a novel MMSE-based receiver design for SC-FDE. Although most of the current literature on SC-FDE is limited to point-to-point systems, there have been recent results reported on FDE in the context of cooperative scenarios [3, 4]. distributed (D)-STBC SC-FDE has been discussed in [3], assuming the maximum likelihood sequence detection (MLSD) equalization. Although significant diversity gains were demonstrated, the complexity of MLSD equalizers increases with the channel memory, signal constellation size, and the number of transmit/receive antennas. This, in turn, places significant additional computational and power consumption loads on the receiver side. Therefore, low-complexity equalization schemes without sacrificing performance are particularly desirable, especially for cases where the receiver implementation is supposed to be simple and required to operate on a limited battery power.

Building upon the work of [5], we propose a novel reduced-complexity MMSE-based receiver design for D-STBC SC-FDE transmissions. Specifically, we are considering amplify-and-forward (AF) relay networks for cooperative scenarios in which either of source to relay ($S \rightarrow R$) or relay to destination ($R \rightarrow D$) links are frequency selective Rician fading. We justify this assumption, by presuming that the line-of-sight (LOS) path exists for either of ($S \rightarrow R$) or $R \rightarrow D$) links. We show that, by incorporating linear processing techniques, our MMSE-based receiver is able to collect full antenna and multipath diversity gains, leading to significant improvement in performance at nearly no additional complexity. Detailed diversity order analysis and complexity analysis are presented to corroborate the proposed system's outperformance compared to the conventional cooperative MMSE-SC-FDE receiver. Specifically, under the assumption of perfect power control and high signal-to-noise ratio (SNR) for the underlying links and assuming either of $S \rightarrow R$ or $R \rightarrow D$ links to be frequency selective Rician fading, our performance analysis demonstrates that the proposed receiver is able to achieve a maximum diversity order of $\min(L_{SR}, L_{RD}) + L_{SD} + 2$, where L_{SR}, L_{RD}, and L_{SD} are the channel memory lengths for $S \rightarrow R$, $R \rightarrow D$, and $S \rightarrow D$ links, respectively. Complexity analysis and simulation results demonstrate that within the bounds of the aforementioned system modeling and assumptions, our proposed receiver outperforms the conventional cooperative MMSE-SC-FDE receiver by performing close to matched filter bound (MFB).

In chapter 5, we investigate the performance of D-STBC SC-FDE systems with AF relaying over frequency-selective Rician fading channels in multi-relay networks. Our performance analysis demonstrates that SC-FDE for DSTBC is able to achieve a maximum

diversity order of $\sum_{i=1}^{R} \min(L_{SR_i}, L_{R_iD}) + R$, where R is the number of participating relays, L_{SR_i} and L_{R_iD} are the channel memory lengths for source to i^{th} relay ($S \rightarrow R_i$) link and i^{th} relay to destination ($R_i \rightarrow D$) link , respectively. Simulation results are provided to corroborate the theoretical analysis.

Finally, we summarize the work in this thesis and present the conclusions in Chapter 6.

1.3 Notations and Acronyms

In this section we define the notations and acronyms used throughout this thesis.

$\mathbf{a}$	A boldface lowercase letter denotes a vector.
$\mathbf{A}$	A boldface uppercase letter denotes a matrix.
$\bar{(.)}$	Conjugate operation.
$(.)^{\mathrm{T}}$	Transpose operation.
$(.)^{\mathrm{H}}$	Hermitian transpose operation.
$(.)^{-1}$	Inverse operation.
$[.]_{k,l}$	$(k,l)^{th}$ entry of a matrix.
$[.]_k$	k^{th} entry of a vector.
$\mathbf{I}_N$	identity matrix of size N.
$\mathbf{0}_{M\times M}$	all-zero matrix of size $M \times M$.
P_N	$N \times N$ permutation matrix.
$[\mathrm{P}_N^q \mathbf{a}]_s$	$\mathbf{a}\,((N-s+q) \bmod N)$, for $\mathbf{a} = [\ a_0 \quad \cdots \quad a_{N-1}]^{\mathrm{T}}$.
$\mathbf{Q}$	$N \times N$ FFT matrix with $\mathbf{Q}(l,k) = 1/\sqrt{N}\exp(-j2\pi lk/N)$.

Table 1.1: List of notations.

2G	second-generation
3G	third-generation
4G	fourth-generation
AF	amplify-and-forward
AWGN	additive white Gaussian noise
BER	bit error rate
CIR	channel impulse response
C-OFDM	coded OFDM
CP	cyclic prefix
CSI	channel state information
DAB/DVB	digital audio/video broadcasting
DF	decode-and-forward
DFT	discrete Fourier transform
DSL	digital subscriber lines
D-STBC	distributed space-time block coded
EGC	equal gain combining
FD	frequency domain
FDE	frequency domain equalization
FFT	fast Fourier transform
FIR	finite impulse response
IBI	inter-block interference
IFFT	inverse fast Fourier transform
ISI	intersymbol interference
LAN	local area networks
LCP-OFDM	linear constellation precoded OFDM
LDC	linear dispersion codes
LOS	line-of-sight
MFB	matched filter bound
MIMO	multiple-input-multiple-output
MISO	multiple-input-single-output
ML	maximum likelihood
MLSD	maximum likelihood sequence detection

MMSE	minimum mean square error
MRC	maximal ratio combining
NAF	non-orthogonal amplify-and-forward
OFDM	orthogonal frequency division multiplexing
OFDMA	orthogonal frequency-division multiple access
pdf	probability density function
PAR	peak-to-average ratio
PEP	pairwise error probability
PSK	phase-shift keying
QAM	quadrature amplitude modulation
SC	selection combining
SC	single carrier
SER	symbol error rate
SIMO	single-input-multiple-output
SNR	signal-to-noise ratio
SO-STTC	super-orthogonal space-time trellis coding
SR	selection relaying
STBC	space-time block codes
STTCs	space-time trellis codes
TCM	trellis-coded modulation
TD	time domain
TDMA	time-division multiple access
WPANs	wireless personal area network
WSN	wireless sensor networks
ZP	zero padding

Table 1.2: List of acronyms.

Chapter 2

Background

2.1 Introduction

A glimpse of recent technological history reveals out that mobile communication systems create a new generation roughly every 10 years. First-generation analogue systems were introduced in the early 1980's, then second-generation (2G) digital systems came in the early 1990's. Later, third-generation (3G) systems gradually unfolded all over the world while intensive conceptual and research work toward the definition of a future system had been already started.

2G systems, such as GSM and IS-95, were essentially designed for voice and low data rate applications. In an effort to address customer demands for high-speed data communication, telecommunication companies have been launching 3G systems where the business focus has shifted from voice services to multimedia communication applications over the Internet. Despite the increasing penetration rate of 3G systems in the wireless market, 3G networks are challenged primarily in meeting the requirements imposed by the ever-increasing demands of high-throughput multimedia and internet applications. Additionally, 3G systems consist primarily of wide area networks and thus fall short of supporting heterogeneous networks, including wireless local area networks (LANs) and wireless personal area networks (WPANs).

Several wireless technologies co-exist in the current market customized for different service types, data rates, and users. The next generation systems also known as the fourth generation (4G) systems are envisioned to accommodate and integrate all existing and future technologies in a single standard. The key feature of the 4G systems would be "high

usability" [6]; that is the user would be able to use the system at anytime, anywhere, and with any technology. Users carrying an integrated wireless terminal would have access to a variety of multimedia applications in a reliable environment at lower cost. To meet these demands, next generation wireless communication systems must support high capacity and variable bit rate information (adaptive) transmission with high bandwidth efficiency to conserve limited spectrum resources.

2.2 Diversity Techniques for Fading Channels

The characteristics of the wireless channel impose fundamental limitations on the performance of wireless communication systems. The wireless channel can be investigated by decomposing it into two parts, i.e., large-scale (long-term) impairments including path loss, shadowing and small-scale (short-term) impairment which is commonly referred as fading. The former component is used to predict the average signal power at the receiver and the transmission coverage area. The latter is due to the multipath propagation which causes random fluctuations in the received signal level and affects the instantaneous SNR.

For a typical mobile wireless channel in urban areas where there is no LOS propagation and the number of scatters is large, the application of central limit theory indicates that the complex fading channel coefficient has two quadrature components which are zero-mean Gaussian random processes. As a result, the amplitude of the fading envelope follows a Rayleigh distribution. In terms of error rate performance, Rayleigh fading converts the exponential dependency of the bit-error probability on the SNR for the additive white Gaussian noise (AWGN) channel into an approximately inverse linear one, resulting in a large SNR penalty.

A common approach to mitigate the degrading effects of fading is the use of diversity techniques. Diversity improves transmission performance by making use of more than one independently faded versions of the transmitted signal. If several replicas of the signals are transmitted over multiple channels that exhibit independent fading with comparable average strengths, the probability that all the independently faded signal components experience deep fading simultaneously is significantly reduced.

There are various approaches to extract diversity from the wireless channel. The most common methods are briefly summarized as follows [7, 8, 9]:

2.2.1 Time Diversity

In this form of diversity, the same signal is transmitted in different time slots separated by an interval longer than the coherence time of the channel. Channel coding in conjunction with interleaving is an efficient technique to provide time diversity. In fast fading environments where the mobility is high, time diversity becomes very efficient. However, for slow-fading channel (e.g., low mobility environments, fixed-wireless applications), it offers little protection unless significant interleaving delays can be tolerated.

2.2.2 Frequency Diversity

In this form of diversity, the same signal is sent over different frequency carriers, whose separation must be larger than the coherence bandwidth of the channel to ensure independence among diversity channels. Since multiple frequencies are needed, this is generally not a bandwidth-efficient solution. A natural way of frequency diversity, which is sometimes referred to as path diversity, arises for frequency-selective channels. When the multipath delay spread is a significant fraction of the symbol period, the received signal can be interpreted as a linear combination of the transmitted signal weighted by independent fading coefficients. Therefore, path diversity is obtained by resolving the multipath components at different delays using a RAKE correlator [7], which is the optimum receiver in the MMSE sense designed for this type of channels.

2.2.3 Space Diversity

In this form of diversity, which is also sometimes called as antenna diversity, the receiver and/or transmitter uses multiple antennas. This technique is especially attractive since it does not require extra bandwidth. To extract full diversity advantages, the spacing between antenna elements should be wide enough with respect to the carrier wavelength. The required antenna separation depends on the local scattering environment as well as on the carrier frequency. For a mobile station which is near the ground with many scatters around, the channel decorrelates over shorter distances, and typical antenna separation of half to one carrier wavelength is sufficient. For base stations on high towers, a larger antenna separation of several to tens of wavelengths may be required.

2.2.4 Diversity Combining Techniques

There exist different combining techniques, each of which can be used in conjunction with any of the aforementioned diversity forms. The most common diversity combining techniques are selection, equal gain and maximal ratio combining [7]. Selection combining (SC) is conceptually the simplest; it consists of selecting at each time, among the available diversity branches (channels), the one with the largest value of SNR. Since it requires only a measure of the powers received from each branch and a switch to choose among the branches, it is relatively easy to implement. However, the fact that it disregards the information obtained from all branches except the selected one indicates its non-optimality. In equal gain combining (EGC), the signals at the output of diversity branches are combined linearly and the phase of the linear combination are selected to maximize the SNR disregarding the amplitude differences. Since each branch is combined linearly, compared to SC, EGC performs better. In maximal-ratio-combining (MRC), the signals at the output of diversity branches are again combined linearly and the coefficients of the linear combination are selected to maximize the SNR regarding both the phase and the amplitude. The MRC outperforms the other two, since it makes use of the both fading amplitude and phase information. However, the difference between EGC and MRC is not considerably large in terms of power efficiency; therefore, EGC can be preferred where implementation costs are crucial. It should be emphasized that the effectiveness of any diversity scheme rests on the availability of independently faded versions of the transmitted signal so that the probability of two or more versions of the signal undergoing a deep fade is minimum. The reader can refer to [7, 8, 9] and references therein for a broad overview of diversity combining systems.

2.3 Transmit Diversity

Space diversity, in the form of multiple antenna deployment at the receive side, has been successfully used in uplink transmission (i.e., from mobile station to base station) of the cellular communication systems [10]. However, the use of multiple receive antennas at the mobile handset in the downlink transmission (i.e., from base station to mobile station) is more difficult to implement because of size limitations and the expense of multiple down-conversion of RF paths [11]. This motivates the use of multiple transmit antennas at the base station in the downlink. Since a base station often serves many mobile stations, it is also more economical to add hardware and additional signal processing to base stations

rather than the mobile handsets. Despite its obvious advantages, transmit diversity has traditionally been viewed as more difficult to exploit, in part because the transmitter is assumed to know less about the channel than the receiver and in part because of the challenging signaling design problem. Within the last decade, transmit diversity has attracted a great attention and practical solutions to realize transmit diversity advantages have been proposed [9].

The transmit diversity techniques can be classified into two broad categories based on the need for channel state information at the transmit side: Close loop schemes and open loop schemes. The first category uses feedback, either explicitly or implicitly, from the receiver to the transmitter to configure the transmitter. Close loop transmit diversity has more power efficiency compared to open loop transmit diversity. However, it increases the overhead of transmission and therefore is not bandwidth-efficient. Moreover, in practice, vehicle movements or interference causes a mismatch between the state of the channel perceived by the transmitter and that perceived by the receiver, making the feedback unreliable in some situations.

In open loop transmit diversity schemes, feedback is not required. They use linear processing at the transmitter to spread the information across multiple antennas. At the receive side, information is recovered by either linear processing or maximum-likelihood decoding techniques. The first of such schemes was proposed by Wittneben [12, 13] where the operating frequency-flat fading channel is converted intentionally into a frequency-selective channel to exploit artificial path diversity by means of a maximum-likelihood decoder. It was later shown in [14] that delay diversity schemes are optimal in providing diversity in the sense that the diversity advantage experienced by an optimal receiver is equal to the number of transmit antennas.

The linear filtering used to create delay diversity at the transmitter can be viewed as a channel code which takes binary or integer input and creates real valued output. Therefore, from a coding perspective, delay diversity schemes correspond to repetition codes and lead to the natural question as to whether more sophisticated codes might be designed. The challenge of designing channel codes for multiple-antenna systems has led to the introduction of so-called space-time trellis codes by Tarokh, Seshadri and Calderbank [15].

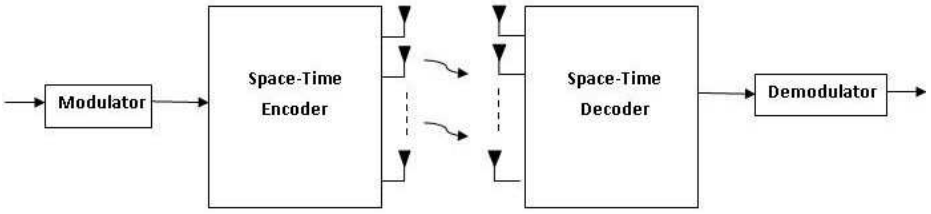

Figure 2.1: Block diagram of a space-time coded system.

2.4 Space-Time Coding

Space-time trellis codes (STTCs) combine the channel code design with symbol mapping onto multiple transmit antennas. The data symbols are cleverly coded across space and time to extract diversity advantages [15]. Figure 2.1 illustrates a space-time coded system. Let space-time code be represented as a $W \times M_S$ matrix, where M_S is the number of transmit antennas and W is the codeword length. Each entry of X represents the modulation symbol transmitted from the m_S^{th} ($m_S = 1, 2, ...M_S$) antenna during the w^{th} ($w = 1, 2, ...W$) symbol period.

$$\mathbf{X} = \begin{bmatrix} x_1^1 & x_2^1 & ... & x_{M_S}^1 \\ x_1^2 & ... & ... & x_{M_S}^2 \\ : & ... & ... & : \\ x_1^W & x_2^W & ... & x_{M_S}^W \end{bmatrix} \tag{2.1}$$

The signal at each receive antenna is a superposition of the M_S transmitted signals corrupted by fading. The received signal at the n^{th} antenna within the w^{th} symbol period is given by

$$r_n^w = \sum_{m_S=1}^{M_S} h_{m_S}^n x_{m_S}^w + n_n^w \tag{2.2}$$

where $h_{m_S}^n$ denotes the frequency flat fading coefficient from the ${m_S}^{th}$ transmit antenna to the n^{th} receive antenna, that is considered to be quasi static constant over the codeword's length W. It is modeled as a complex Gaussian random variable with variance 0.5 per dimension leading to the well-known Rayleigh fading channel model. In (2.2), n_n^w models the additive noise term and is zero-mean complex Gaussian random variable with variance $N_0/2$ per dimension. In matrix notation, the received signal can be written as

$$\mathbf{R} = \mathbf{XH} + \mathbf{N} \tag{2.3}$$

where $\mathbf{R}$ is the received signal matrix of size $W \times N$, N is the number of receive antennas, $\mathbf{H}$ is the channel matrix of size $M_S \times N$, and $\mathbf{N}$ is the additive noise matrix of size $W \times N$. With coherent detection and perfect channel state information (CSI), i.e., the fading coefficients are perfectly estimated and made available to the receiver, the maximum likelihood (ML) receiver depends on the minimization of the metric

$$\hat{\mathbf{X}} = \arg\min_{\mathbf{X}} \|\mathbf{R} - \mathbf{XH}\|^2 \tag{2.4}$$

The ML receiver decodes in favor of another codeword $\hat{\mathbf{X}}$ and let $P\left(\mathbf{X}, \hat{\mathbf{X}}\right)$ denote the pairwise error probability (PEP) which represents the probability of choosing $\hat{\mathbf{X}}$ when indeed $\mathbf{X}$ was transmitted. PEP is the building block for the derivation of union bounds to the error probability. It is widely used in the literature to predict the attainable diversity order where the closed-form error probability expressions are unavailable. In [15], Tarokh et al. derive a Chernoff bound on the PEP for space-time coded systems given by

$$P(\mathbf{X}, \hat{\mathbf{X}}) \leq \left(\prod_{j=0}^{r} \lambda_j\right) \left(\frac{E_S}{4N_0}\right)^{-rN} \tag{2.5}$$

where E_S is the average symbol energy, r is the rank of the codeword difference matrix defined by $\mathbf{E} = \left(\mathbf{X} - \hat{\mathbf{X}}\right)\left(\mathbf{X} - \hat{\mathbf{X}}\right)^{\mathrm{H}}$, and λ_j denotes the non-zero eigenvalues of $\mathbf{E}$. In (2.5), rN represents the diversity advantage, (i.e., the slope of the performance curve), while the product of the non-zero eigen values of $\mathbf{E}$ denotes the coding advantage, (i.e., the horizontal shift of the performance curve). The design criteria for space-time codes are further given in [15]:

Rank criterion: The code difference matrix, taken over all possible combinations of code matrices, should be full rank. This criterion maximizes the diversity gain obtained from the space-time code. The maximum diversity order that can be achieved is $r = \min(W, M_S)$. Therefore, in order to achieve the maximum diversity of $M_S \times N$, $\mathbf{E}$ must be full rank.

Determinant criterion: The minimum determinant of E, taken over all possible combinations of code matrices, should be maximized. This maximizes the coding gain. From (2.5), it can be seen that the diversity gain term dominates the error probability at high

SNR. Therefore, the diversity gain should be maximized before the coding gain in the design of a space-time code.

Based on the above criteria, Tarokh et al. [15] proposed some handcrafted codes which perform very well, within the 2-3 dB of the outage capacity derived in [16] for multiple antenna systems. Since Tarokh's pioneering work, there has been an extensive research effort in this area for the design of optimized space-time trellis codes, a few to name are [17, 18, 19] among many others.

Since every STTC has a well-defined trellis structure, standard soft decision techniques, such as a Viterbi decoder, can be used at the receiver. For a fixed number of transmit antennas, the decoding complexity of STTCs (measured by the number of trellis states at the decoder) increases exponentially with the transmission rate. Space-time block codes (STBCs) [20, 21, 10] were proposed as an attractive alternative to its trellis counterpart with a much lower decoding complexity. These codes are defined by a mapping operation of a block of input symbols into the space and time domains, transmitting the resulting sequences from different antennas simultaneously. Tarokh et al.'s work in [20] was inspired by Alamouti's early work [10], where a simple two-branch transmit diversity scheme was presented and shown to provide the same diversity order as MRC with two receive antennas. Alamouti's scheme is appealing in terms of its performance and simplicity. It requires a very simple decoding algorithm based only on linear processing at the receiver. STBCs based on orthogonal designs [20] generalizes Alamouti's scheme to an arbitrary number of transmit antennas still preserving the decoding simplicity and are able to achieve the full diversity at full transmission rate for real signal constellations and at half rate for complex signal constellations such as QAM or PSK. Over the last few years several contributions have been made to further improve the data rate of STBCs, e.g., [22, 23] and the references therein.

Super-orthogonal space-time trellis coding (SO-STTC) [24] is another class of space-time code family. It combines set-partitioning with a super set of orthogonal STBC. While providing full-diversity and full-rate, the structure of these new codes allows the coding gain to be improved over traditional STTC constructions. The underlying orthogonal structure of these codes can be further exploited to decrease the decoding complexity in comparison to original STTC designs. Another class of space-time codes is linear dispersion codes (LDC) [25]. Original LDCs were originally designed to maximize capacity gains and subsume spatial multiplexing, which is a transmission technique offering a linear (in the number of

transmit-receive antenna pairs) increase in the transmission rate (or capacity) for the same bandwidth and with no additional power expenditure, and STBCs as special cases. This code family is able to provide an efficient trade-off between multiplexing and diversity gains for arbitrary numbers of transmit and receive antennas [26].

As evidenced by the explosion of research papers on the topic, space-time coding and its various combinations are becoming well understood in the research community. A detailed treatment of space-time coding can be found in recently published text-books, e.g., [27, 28, 29].

2.5 Cooperative Diversity

Space-time coding techniques are quite attractive for deployment in the cellular applications at base stations and have been already included in the 3rd generation wireless standards. Although transmit diversity is clearly advantageous on a cellular base station, it may not be practical for other scenarios. Specifically, due to size, cost, or hardware limitations, a wireless device may not be able to support multiple transmit antennas. Examples include mobile terminals and wireless sensor networks which are gaining popularity in recent years.

In order to overcome these limitations, yet still emulate transmit antenna diversity, a new form of realizing spatial diversity has been recently introduced under the name of user cooperation or cooperative diversity [30, 31, 32, 33, 34]. The basic idea behind cooperative diversity rests on the observation that in a wireless environment, the signal transmitted by the source node is overheard by other nodes, which can be defined as "partners" or "relays". The source and its partners can jointly process and transmit their information, creating a virtual antenna array although each of them is equipped with only one antenna. Similar to physical antenna arrays, these virtual antenna arrays combat multipath fading in wireless channels by providing receivers with essentially redundant signals over independent channels that can be combined to average individual channel effects. The recent surge of interest in cooperative communication was subsequent to the works of Sendonaris et al. [30, 31] and Laneman et al. [32, 33, 34]. However, the basic ideas behind user cooperation can be traced back to Meulen's early work on the relay channel [35]. A first rigorous information theoretical analysis of the relay channel has been introduced in [36] by Cover and Gamal for AWGN channels. Extending the work of [36] for fading channels, Sendonaris et al. [30, 31] have investigated the achievable rate region for relay-assisted transmission and coined the

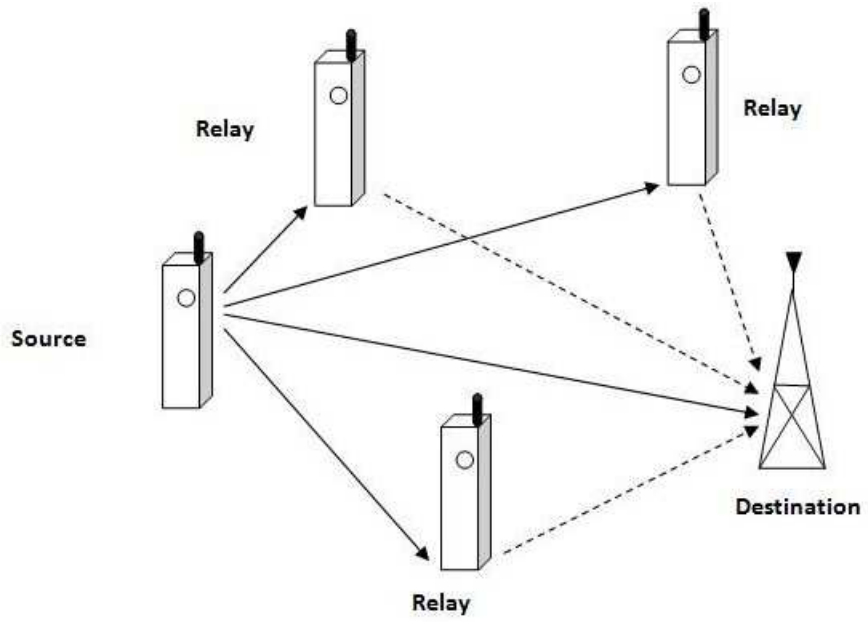

Figure 2.2: Relay assisted transmission.

term "user cooperation".

In an independent work by Laneman et al. [32, 33] it is demonstrated that full spatial diversity can be achieved through user cooperation. Their proposed user cooperation protocol is built upon a two-phase transmission scheme. In the first phase (i.e., broadcasting phase), the source broadcasts to the destination and relay terminals. In the second phase (i.e., relaying phase), the relays transmit processed version of their received signals to the destination using either orthogonal subchannels, i.e., repetition based cooperative diversity, or the same subchannel, i.e., space-time coded cooperative diversity. The latter relies on the implementation of conventional orthogonal space-time block coding [15] in a distributed fashion among the relay nodes.

Two main relaying techniques are studied in [32]: AF and Decode-and-Forward (DF). In DF relaying, the relay node fully decodes, re-encodes and re-transmits the source node's message. In AF relaying, the relay retransmits a scaled version of the received signal without any attempt to decode it. AF relaying can be furthered categorized based on the availability of CSI at the relay terminal. In CSI-assisted AF scheme [32], the relay uses instantaneous CSI of the source to relay ($S \rightarrow R$) link to scale its received noisy signal before re-transmission. This ensures that the same output power is maintained for each

realization. On the hand, the "blind" AF scheme does not have access to CSI and employs fixed power constraint. This ensures that an average output power is maintained, but allows for the instantaneous output power to be much larger than the average. Although blind AF is not expected to perform as well as CSI-assisted AF relaying, the elimination of channel estimation at the relay terminal promises low complexity and makes it attractive from a practical point of view.

Another classification for relaying is also proposed in [32]. In the so-called "fixed" relaying, the relay always forwards the message that it receives from the source. The performance of fixed DF relaying is limited by direct transmission between the source and relay. An alternative to fixed relaying is "selection" relaying (SR) which is, in nature, adaptive to the channel conditions. In this type of relaying, the source reverts to non-cooperation mode at times when the measured instantaneous SNR falls below a certain threshold and continues its own direct transmission to the destination. The work in [37, 38] can be considered as a systematic realization of such adaptive relaying through powerful channel coding techniques. In so-called "coded cooperation" of [37, 38], Hunter et al. realize the concept of user cooperation through the distributed implementation of existing channel coding methods such as convolutional and turbo codes. The basic idea is that each user tries to transmit incremental redundancy for its partner. Whenever that is not possible, the users automatically revert to a non-cooperative mode.

The user cooperation protocol proposed by Laneman et al. in [34] effectively implements transmit diversity in a distributed manner. In [39], Nabar et al. establish a unified framework of cooperation protocols for single-relay wireless networks. They quantify achievable performance gains for distributed schemes in an analogy to conventional co-located multi-antenna configurations. Specifically, they consider three (time-division multiple access) TDMA-based protocols named Protocol I, Protocol II, and Protocol III which correspond to traditional MIMO (multi-input-multi-output), SIMO (single-input-multi-output) and MISO (multi-input -single-output) schemes, respectively (Table 1.1). In the following, we describe these cooperation protocols which will be also a main focus of our work.

- **Protocol I**: During the first time slot, the source terminal communicates with the relay and destination. During the second time slot, both the relay and source terminals communicate with the destination terminal. This protocol realizes maximum degrees of broadcasting and receive collision. In an independent work by Azarian et

al. [40], it has been demonstrated that this protocol is optimum in terms of diversity-multiplexing tradeoff. Protocol I is referred as "non-orthogonal amplify and forward (NAF) protocol" in [40].

- **Protocol II**: The source terminal communicates with the relay and destination terminals in first time slot. In the second time slot, only the relay terminal communicates with the destination. This protocol realizes a maximum degree of broadcasting and exhibits no receive collision. This is the same cooperation protocol proposed by Laneman et al. in [32].

- **Protocol III**: This is essentially similar to Protocol I except that the destination terminal does not receive from the source during the first time slot. This protocol does not implement broadcasting but realizes receive collision.

Table 2.1: Cooperation protocols for single-relay networks.

Protocol \ Terminal	Protocol I		Protocol II		Protocol III	
	Time 1	Time 2	Time 1	Time 2	Time 1	Time 2
Source	●	●	●	–	●	●
Relay	○	●	○	●	○	●
Destination	○	○	○	○	–	○

●: Transmitting, ○: Receiving, –: Idle

2.6 Orthogonal frequency division multiplexing

The goal for people to have access to the capabilities of the global network at any time, irrespective of the mobility and location, has become increasingly achievable, thanks to the tremendous growth in wireless communication over the last two decades [41]. Moreover, the increasing demand for wireless multimedia and interactive Internet services has led to intensive research efforts on high speed data transmission. Unfortunately, unlike wireline communication, there are crucial obstacles to wireless communications. Firstly, the radio spectrum resources are very limited and expensive. Secondly, due to the harsh wireless environment, signals may undergo rapid fluctuations caused by multipath propagation when

going through wireless channels [42, 7]. Therefore, the most desirable communication techniques in this era, are those to improve the quality and spectral efficiency of the wireless communication links.

A key challenge for high-speed broadband applications is the dispersive nature of frequency-selective fading channels, which causes the so-called intersymbol interference (ISI), leading to performance degradation.

To mitigate the ISI phenomenon, OFDM was proposed as an anti-multipath multicarrier modulation scheme. OFDM is a multicarrier technique in which the transmitted bitstream is divided into many different substreams and sent over many different subchannels, which are orthogonal under ideal propagation conditions. The data rate on each of the subchannels is much less than the total data rate, and the corresponding subchannel bandwidth is much less than the total system bandwidth. The number of substreams is chosen to ensure that each subchannel has a bandwidth less than the coherence bandwidth of the channel, so that the subchannels experience relatively flat fading. This implementation, makes the ISI on each subchannel small [43]. Note that the channel affects only the phase and amplitude of the subcarrier and therefore, equalizing each subcarrier's phase and gain, will compensate for the frequency selective fading.

In order to generate the multiple subcarriers, the inverse fast Fourier transform (IFFT) is performed at the transmitter side on blocks of M data symbols. Note that the fast Fourier transform (FFT) block length M is at least 4-10 times longer than the maximum impulse response span, mainly to minimize the fraction of overhead due to the insertion of the cyclic prefix (CP) at the beginning of each block. Cyclic prefix is the repetition of the last data symbols in a block and it serves two goals [44]: firstly, it prevents contamination of a block by ISI from previous blocks. secondly, it makes the received block appear to be periodic with period M. Note that the periodicity of the received block, produces circular convolution, which is essential to the proper functioning of FFT.

2.7 Single-carrier frequency domain equalization

An SC system transmits a modulated single carrier at a high symbol rate and is basically the frequency domain analog of what is done by conventional linear time domain equalizers. Note that FDE is performed on a block of data at a time, where the operations on this block involve an efficient FFT operation and a simple channel inversion operation, that makes it

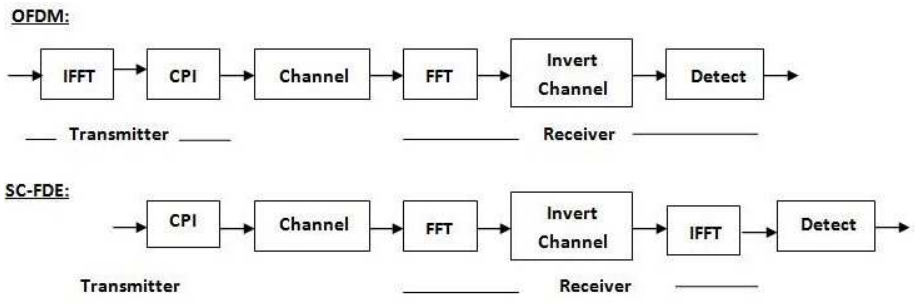

Figure 2.3: OFDM and SC-FDE– signal processing similarities and differences.

computationally simpler than the corresponding TD equalization, for channels with severe delay spreads. Therefore, the SC system with FDE (SC-FDE) has essentially the same performance and low complexity as OFDM, when combined with FFT processing and the use of cyclic prefixing [45].

2.8 Summary

This chapter has covered different areas of wireless communication, knowledge of which is essential to the rest of the thesis. These subjects include diversity techniques for fading channels, transmit diversity techniques, space-time coding, cooperative diversity, multicarrier modulation techniques, OFDM, SC-FDE, and SC-STBC-FDE.

Chapter 3

A New Detection Scheme for Zero-Padded OFDM

3.1 Introduction

Recently, ZP-OFDM has been proposed as an alternative solution to coded-OFDM, which often incurs high decoding complexity. Various ZP-OFDM receivers have been proposed in the literature, trading off performance with complexity. In this chapter, we propose a novel low-complexity receiver for ZP-OFDM transmissions. We demonstrate that the proposed receiver brings a significant complexity reduction in the receiver design, while outperforming conventional MMSE-ZP-OFDM.

3.2 Overview

The growing demand for high data rate services for wireless multimedia and internet services has lead to intensive research efforts on high speed data transmission. A key challenge for high-speed broadband applications is the dispersive nature of frequency-selective fading channels, which causes the so-called ISI leading to an inevitable performance degradation. An efficient approach to mitigate ISI is the use of OFDM which converts the ISI channel with AWGN into parallel ISI-free subchannels by implementing IFFT at the transmitter and FFT at the receiver side [46]. It has been shown that OFDM is an attractive equalization scheme for digital audio/video broadcasting (DAB/DVB) [47], and it has successfully been applied to high-speed modems over digital subscriber lines (DSL) [48]. Recently, it has also

been proposed for broadband television systems and mobile wireless local area networks such as IEEE802.11a and HIPERLAN/2 (HL2) standards [1].

The IFFT precoding at the transmitter side and insertion of CP enable OFDM with very simple equalization of frequency-selective finite impulse response (FIR) channels. To avoid InterBlock Interfernce (IBI) between successive FFT processed blocks, the CP is discarded and the truncated blocks are FFT processed so that the frequency-selective channels are converted into parallel flat-faded independent subchannels. In this way, the linear channel convolution is converted into circular convolution and the receiver complexity both in equalization and the symbol decoding stages is reduced [49]. However, since each symbol is transmitted over a single flat subchannel, the multipath diversity is lost along with the fact there is no guarantee for symbol delectability when channel nulls occur in the subchannels. As an additional counter-measure, coded OFDM (C-OFDM), which is fading resilient, has been adopted in many standards [50]. Trellis-coded modulation (TCM) [51] and convolutional codes [52, 53] are typical choices for error-control codes. Interleaving together with TCM enjoys low complexity Viterbi decoding while enabling a better trade off between bandwidth and efficiency. However, designing systems that achieve diversity gain equal to code length is difficult considering the standard design paradigms for TCM. Linear constellation precoded OFDM (LCP-OFDM) was further proposed in [54] to improve performance over fading channels, where a real orthogonal precoder is applied to maximize the minimum product distance [55, 56] and channel cutoff rate [57], while maintaining the transmission rate and guaranteeing the symbol recovery. Subcarrier grouping was proposed in [54] to enable the maximum possible diversity and coding gain. However, the LCP that is used within each subset of subcarriers is in general complex.

To ensure symbol recovery regardless of channel nulls, ZP of multicarrier transmission has been proposed to replace the generally non-zero CP. Unlike CP-OFDM, ZP-OFDM guarantees symbol recovery and FIR equalization of FIR channels. Specifically, the zero symbols are appended after the IFFT processed information symbols. In such way, the single FFT required by CP-OFDM is replaced by FIR filtering in ZP-OFDM which adds to the receiver complexity. To trade-off BER performance for extra savings in complexity, two low complexity equalizers for ZP-OFDM are derived in [1]. Both schemes are developed based on the circularity of channel matrix while reducing complexity by avoiding inversion of a channel dependent matrix. However, the BER performance of the two sub-optimal receivers proposed in [1] is not as good as MMSE-ZP-OFDM.

In this chapter, we propose a novel reduced complexity receiver design for ZP-OFDM transmissions that not only outperforms MMSE-ZP-OFDM, but also uses low-complexity computational methods that bring a significant power saving to the proposed receiver. This makes it a strong candidate for WSNs which are characterized by small and low-power devices. We show that linear processing collects both multipath and spatial diversity gains, leading to significant improvement in performance, while maintaining low complexity.

3.3 System Model

We consider a single transmit single receive antenna system over a frequency-selective fading wireless channel. The (channel impulse response) CIR of the jth information block is modeled as an FIR filter with coefficients $\mathbf{h}^j = \left[h^j[0], ..., h^j[L]\right]^{\mathrm{T}}$, where L denotes the corresponding channel memory length. The random vectors $\mathbf{h}^j$ are assumed to be independent zero-mean complex Gaussian with two choices of power delay profile: uniform power delay profile with variance $1/(L+1)$; and exponentially decaying power-delay profile $\theta(\tau_k) = Ce^{-\tau_k/\tau_{rms}}$ with delays τ_k that are uniformly and independently distributed [58].

The jth $M \times 1$ information block $\mathbf{x}_M^j$ is padded by D trailing zeros and IFFT precoded by the IFFT matrix to yield the time-domain block vector $\tilde{\mathbf{x}}_{zp}^j$

$$\tilde{\mathbf{x}}_{zp}^j = \mathbf{Q}_{zp}\mathbf{x}_M^j, \tag{3.1}$$

where

$$\mathbf{Q}_{zp} = [\mathbf{Q}_M \mathbf{0}_{D\times M}]^H. \tag{3.2}$$

Therefore, the received block symbol is given by

$$\tilde{\mathbf{r}}_{zp}^j = \mathbf{H}\mathbf{Q}_{zp}\mathbf{x}_M^j + \mathbf{H}_{IBI}\mathbf{Q}_{zp}\mathbf{x}_M^{j-1} + \tilde{\mathbf{n}}_N^j, \tag{3.3}$$

where $N = M + D$; $\mathbf{H}$ is the $N \times N$ lower triangular Toeplitz filtering matrix with its first column being $\begin{bmatrix} h^j[0], ..., h^j[L] & 0, ..., 0 \end{bmatrix}^{\mathrm{T}}$; $\mathbf{H}_{IBI}$ is the $N \times N$ upper triangular Toeplitz filtering matrix that captures the (inter block interference) IBI, with its first row being $\begin{bmatrix} 0, ..., 0 & h^j[0], ..., h^j[L] \end{bmatrix}$; and $\tilde{\mathbf{n}}_N^j$ denotes the AWGN noise. Having $\mathbf{H}_{IBI}\mathbf{Q}_{zp} = 0$, the all-zero $\mathbf{0}_{D\times M}$ matrix plays the key role in ZP-OFDM by eliminating the IBI. Having the $\mathbf{H}$

matrix partitioned between its first M and last D columns as $\mathbf{H} = [\mathbf{H}_0, \mathbf{H}_{zp}]$, the received block symbol will be given by

$$\tilde{\mathbf{r}}_{zp}^{j} = \mathbf{H}\mathbf{Q}_{zp}\mathbf{x}_M^j + \tilde{\mathbf{n}}_N^j = \mathbf{H}_0\mathbf{Q}_M^H\mathbf{x}_M^j + \tilde{\mathbf{n}}_N^j. \tag{3.4}$$

The $N \times M$ submatrix $\mathbf{H}_0$, which corresponds to the first M columns of $\mathbf{H}$, is Toeplitz and is guaranteed to be invertible, which assures symbol recovery regardless of channel zero locations. In this case, owing to its channel-irrespective symbol delectability property, ZP-OFDM is able to exploit fully the underlying multipath diversity [46]. Assuming variance $\sigma_x^2 = 1$ for the symbols, the MMSE equalizer for additive white Gaussian noise of variance σ_n^2 is given by [1]

$$\mathbf{G}_{mmse} = \mathbf{Q}_M\mathbf{H}_0^H(\sigma_n^2\mathbf{I}_N + \mathbf{H}_0\mathbf{H}_0^H)^{-1}. \tag{3.5}$$

It should be emphasized that channel inversion of an $N \times N$ matrix is costly to be precomputed due to its dependence on the channel. This brings about an extra implementation cost for the MMSE-ZP-OFDM receiver. To overcome this limitation, our proposed scheme targets practical ZP-OFDM receiver that exploits full multipath diversity.

3.4 Reduced complexity MMSE-based receiver

The proposed receiver illustrated in Fig. 3.1 given in page 33, includes a suboptimal channel independent MMSE equalizer in the feed forward stage, followed by linear processing operations in the feed-back stage. Specifically, the feed forward stage exploits the circulant structure of the channel matrices,

$$\mathbf{H}' = \mathbf{Q}\mathbf{\Lambda}\mathbf{Q}^H, \tag{3.6}$$

where $\mathbf{H}'$ is an $N \times N$ circulant matrix with entries $[\mathbf{H}']_{k,l} = \mathbf{h}((k-l) \bmod N)$; $\mathbf{\Lambda}$ is a diagonal matrix whose (n,n) element is equal to the n^{th} discrete Fourier transform (DFT) coefficient of $\mathbf{h}$. Owing to the trailing zeros, the last D columns of $\mathbf{H}$ in (3.4) do not affect the received block. Thus, the Toeplitz matrix $\mathbf{H}$ can be replaced by the $N \times N$ circulant matrix $\mathbf{H}'$ and (3.4) can be written as

$$\tilde{\mathbf{r}}_{zp}^{j} = \mathbf{H}\mathbf{Q}_{zp}\mathbf{x}_M^j + \tilde{\mathbf{n}}_N^j = \mathbf{H}'\mathbf{Q}_{zp}\mathbf{x}_M^j + \tilde{\mathbf{n}}_N^j. \tag{3.7}$$

The $\mathbf{H}'$ matrix takes advantage of FFT to yield a set of flat fading channels that can be equalized easily. The ZP-OFDM receiver output will be

$$\mathbf{r}_N^j = \mathbf{Q}_N\mathbf{H}'\mathbf{Q}_{zp}\mathbf{x}_M^j + \mathbf{n}_N^j = \mathbf{Q}_N\mathbf{H}'\mathbf{Q}_N^H\mathbf{Q}_N\mathbf{Q}_{zp}\mathbf{x}_M^j + \mathbf{n}_N^j = \Lambda\mathbf{V}\mathbf{x}_M^j + \mathbf{n}_N^j, \tag{3.8}$$

where

$$\mathbf{V} = \mathbf{Q}_N\mathbf{Q}_{zp}. \tag{3.9}$$

After applying the N-point FFT Q_N to $\tilde{\mathbf{r}}_{zp}^j$, the suboptimal MMSE-ZP-OFDM receiver in the feed forward stage is formed in two steps. First, following [1], we obtain an MMSE estimator of $\mathbf{y}_N^j = \mathbf{V}\mathbf{x}_M^j$ using

$$\hat{\mathbf{y}}_N^j = E[\mathbf{y}_N^j(\mathbf{r}_N^j)^H].E^{-1}[\mathbf{r}_N^j(\mathbf{r}_N^j)^H] = \mathbf{V}\mathbf{V}^H\Lambda^H[\sigma_n^2\mathbf{I} + \Lambda\mathbf{V}\mathbf{V}^H\Lambda^H]^{-1}. \tag{3.10}$$

Assuming that $\mathbf{V}\mathbf{V}^H \approx (P/N)\mathbf{I}$, (3.10) can be further simplified to

$$\hat{\mathbf{y}}_N^j = \mathbf{\Lambda}^H[(N/P)\sigma_n^2\mathbf{I} + \mathbf{\Lambda}\mathbf{\Lambda}^H]^{-1}. \tag{3.11}$$

The resulting data streams detected from (3.11) are fed into a minimum Euclidean distance decoder, yielding $\hat{\mathbf{x}}_M^j$, i.e., a decoded version of the transmitted symbols. The decoded signals are then fed into the feed-back stage, which is responsible for exploiting the underlying multipath diversity. Specifically, consider the generation of the matrix $\mathbf{\Pi}_l$, $l = 0, 1, 2, ..., L$, as follows:

$$[\mathbf{\Pi}_l]_{p,q} = \begin{cases} 0 & p - q \bmod N = l \\ [\mathbf{H}']_{p,q} & p - q \bmod N \neq l \end{cases}, \tag{3.12}$$

where $1 \leq p, q \leq N$, then, (3.7) can be re-written as

$$\tilde{\mathbf{r}}_l' = \tilde{\mathbf{r}}_{zp}^j - \mathbf{\Pi}_l\mathbf{Q}_{zp}\hat{\mathbf{x}}_M^j. \tag{3.13}$$

Under the high SNR assumption, we can safely assume that $\mathbf{x}_M^j \approx \hat{\mathbf{x}}_M^j$. Therefore, we can write (3.13) as follows:

$$\tilde{\mathbf{r}}_l' = \mathbf{H}_l\mathbf{Q}_{zp}\mathbf{x}_M^j + \tilde{\mathbf{n}}_N^j, \tag{3.14}$$

where

$$[\mathbf{H}_l]_{p,q} = \begin{cases} [\mathbf{H}']_{p,q} & p-q \bmod N = l \\ 0 & p-q \bmod N \neq l \end{cases}. \tag{3.15}$$

After taking the FFT of (3.14) we have:

$$\mathbf{z}_l^j = \mathbf{Q}_N \mathbf{H}_l \mathbf{Q}_{zp} \mathbf{x}_M^j + \mathbf{n}_N^j = \mathbf{Q}_N \mathbf{H}_l \mathbf{Q}_N^H \mathbf{Q}_N \mathbf{Q}_{zp} \mathbf{x}_M^j + \mathbf{n}_N^j = \Lambda_l \mathbf{V} \mathbf{x}_M^j + \mathbf{n}_N^j, \tag{3.16}$$

where $\mathbf{H}_l = \mathbf{Q}\mathbf{\Lambda}_l\mathbf{Q}^H$; $\mathbf{\Lambda}_l$ is a diagonal matrix whose n^{th} element is equal to the DFT coefficient of $\mathbf{h}_l^j = [\ 0...0 \quad h^j[l] \quad 0...0\ ]$. Interestingly, the frequency selective channels are now converted in to parallel independent frequency flat channels. The signals $\mathbf{z}_l^j, l = 0, 1, ..., L$, can now be combined, resulting in

$$\tilde{\mathbf{z}}^j = \sum_{l=0}^{L} \mathbf{\Lambda}_l \mathbf{V} \mathbf{x}_M^j + (L+1)\, \mathbf{n}_N^j. \tag{3.17}$$

The signal in (3.17) is then processed by $\mathbf{\Lambda}^\dagger$ and $\mathbf{V}^\dagger$ where $\mathbf{\Lambda} = \sum_{l=0}^{L} \mathbf{\Lambda}_l$ and fed into a maximum likelihood decoder to recover the transmitted symbols. It is observed from (3.17) that the maximum achievable diversity order is given by $L+1$. This illustrates that our proposed receiver is able to fully exploit the underlying spatial and multipath diversity gains relying on simple linear processing operations only.

3.5 Computational Complexity Analysis

In this section, we focus on the computational complexity of the proposed receiver compared to the conventional MMSE-ZP-OFDM receiver. The computational complexity is measured based on the number of the complex multiplications and complex divisions. Since complex divisions can be implemented in various different ways, we did not decompose them into complex multiplication. The overall computational complexity for the proposed receiver and the conventional MMSE-ZP-OFDM receiver are summarized in Table 3.1 for the case of HL2 (M=64 and N=80).

The computational complexity of the proposed receiver versus the MMSE-ZP-OFDM receiver in terms of the number of the complex multiplications, is illustrated in Fig. 3.2,

which is plotted against the number of the received blocks. The complex divisions' complexity is not considered in this figure, mainly because it's negligible compared to the complexity of the complex multiplications. We are assuming that the channel estimate is updated, each time a symbol block is received. We would like to emphasize that the MMSE equalizer in MMSE-ZP-OFDM requires the inversion of an $N \times N$ channel dependent matrix, which has to be computed for each block received with a complexity of the order $O(N^3)$ [59].

It is observed from Fig. 3.2 that the aggregate complexity of the proposed receiver is insignificant compared to the conventional MMSE-ZP-OFDM, as the number of the received blocks increases. Therefore, the proposed receiver is a strong candidate for the energy constrained WSNs, such that, we can minimize the communication power consumption at no additional hardware cost, by applying linear processing techniques with minimum computational complexity.

Table 3.1: Comparison of overall computational complexity in the HL2.

Implementation	Complex Multiplications	Complex Divisions
ZP-OFDM-MMSE	515840 [1, 59]	NONE
Proposed	246144	160

3.6 Numerical Results

In this section, we present Monte-Carlo simulation results for the proposed receiver assuming a quasi-static Rayleigh fading channel. We are assuming that the correct decisions are fed into the feed-back stage i.e. no decision errors. In figures 3.3 and 3.4, the channel impulse responses CIRs are modeled as frequency selective channels with memory lengths $L = 3, 4$ and a uniform power delay profile assuming 16-PSK modulation.

Fig. 3.3 illustrates the symbol error rate (SER) performance of the proposed receiver for L=3. As a benchmark, we also include the performance of the MMSE-ZP-OFDM receiver which was proposed in [60]. It is clear from the slope of the curves that our new receiver is able to collect full diversity gains, i.e., (L+1)=4, confirming our earlier conclusion. Our simulation results indicate that the proposed receiver outperforms the MMSE-ZP-OFDM equalizer by $\approx$ 3.3dB at SER = 10^{-3}.

In Fig. 3.4, we provide further results on the performance of the proposed receiver for L=4. We also include the performance of MMSE-ZP-OFDM as a benchmark. As

can be observed from the slope of the curve, the proposed receiver is able to collect full diversity gains, i.e., (L+1)=5. Our results indicate that the proposed receiver outperforms the MMSE-ZP-OFDM equalizer by 4.5dB at SER = 10^{-3}.

In Fig. 3.5 and Fig. 3.6, the SER performance of the proposed receiver for L=6, 7 are presented with exponential power-delay profile and 16 PSK modulation. In Fig. 3.5 our results indicate that the proposed receiver outperforms the MMSE-ZP-OFDM equalizer by 8dB at SER = 10^{-3}. This performance improvement is 8dB for Fig. 3.6 at SER = 10^{-3}. These results assure of the proposed receiver's SER ourperformance compared to MMSE-ZP-OFDM, for different power delay profile scenarios. Interestingly, it observed from Figs. 3.3, 3.4, 3.5 and 3.6 that performance improvement of the proposed receiver, in comparison to the benchmark, increases as L increases.

3.7 Summary

We propose a novel reduced-complexity MMSE-based receiver for ZP-OFDM systems. We show that, by incorporating linear processing techniques, our MMSE-based receiver is able to collect full antenna and multipath diversity gains. Simulation results demonstrate that our proposed receiver outperforms the conventional MMSE-ZP-OFDM receiver, while providing much less complexity by avoiding channel dependent matrix inversion. By using linear processing techniques that require minimum computational complexity, the communication power is minimized at no additional hardware cost which makes the proposed receiver a strong candidate for the energy constrained WSNs.

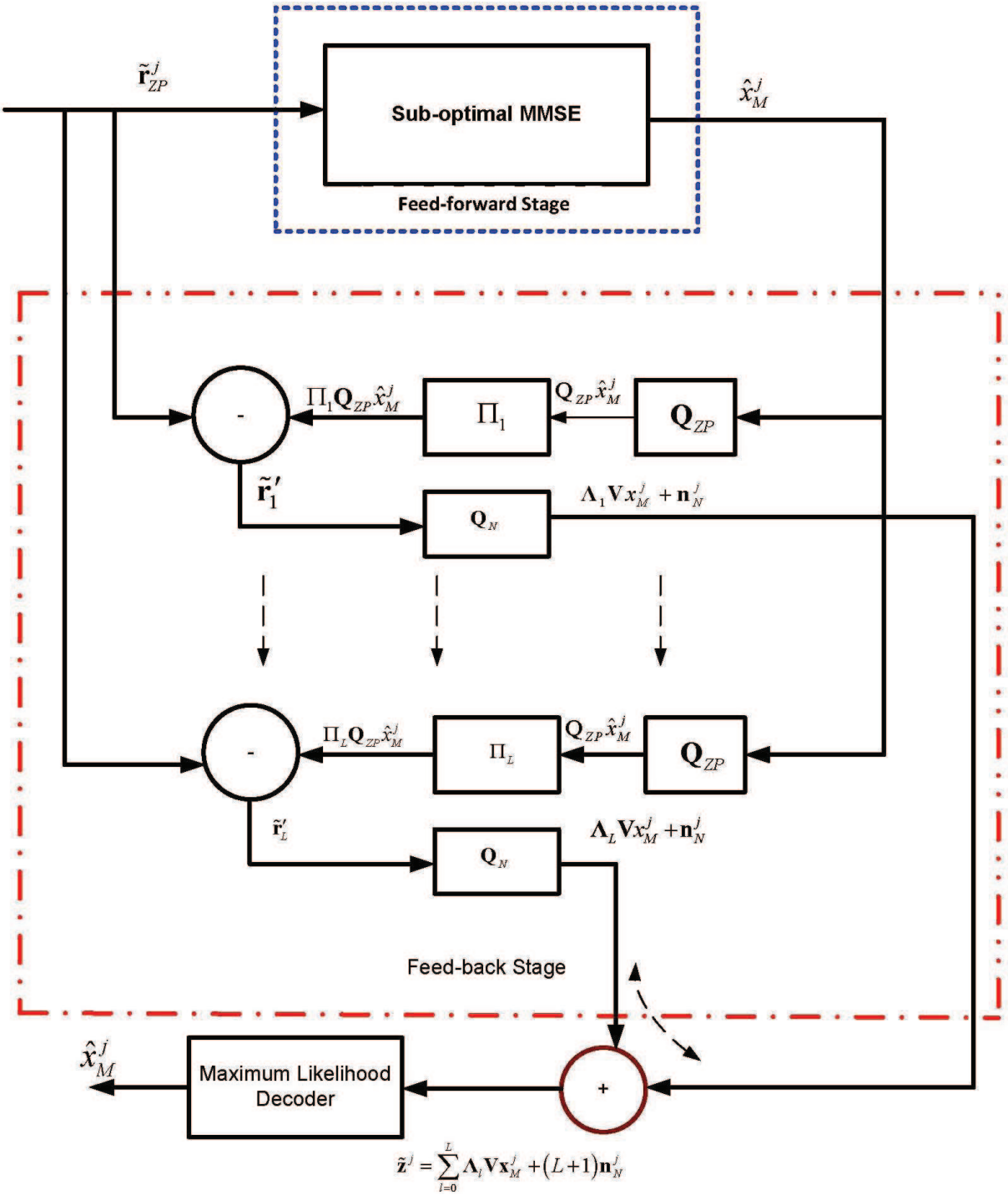

Figure 3.1: Proposed low-complexity MMSE-ZP-OFDM receiver block diagram.

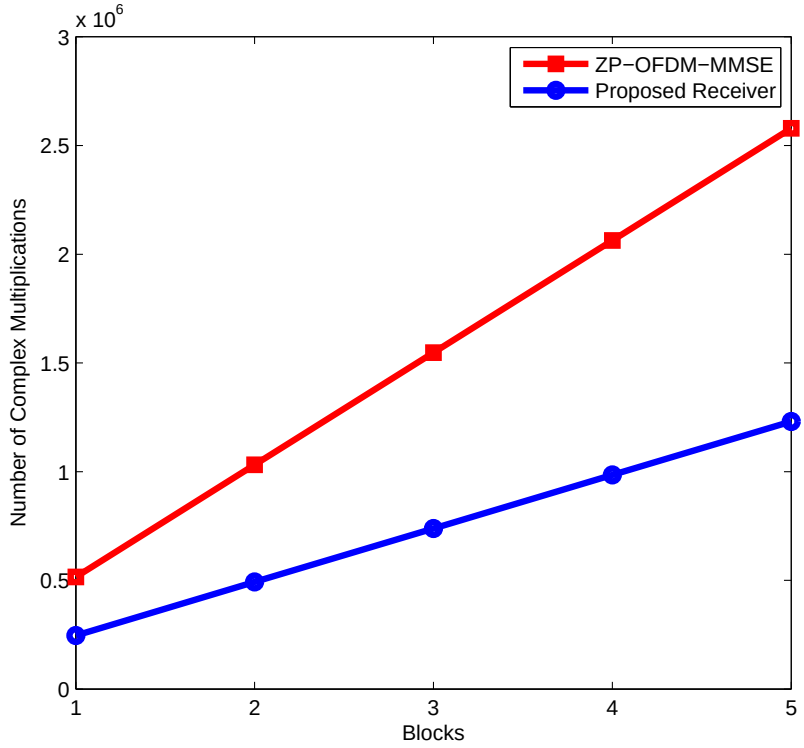

Figure 3.2: Computational complexity of the proposed receiver compared to ZP-OFDM-MMSE.

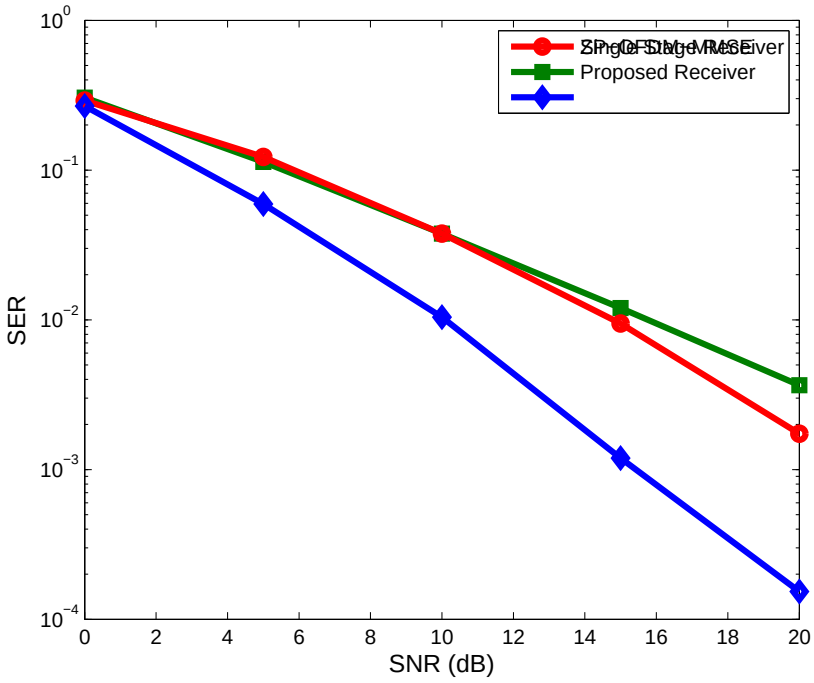

Figure 3.3: BER performance of ZP-OFDM-MMSE, single stage receiver and proposed receiver, uniform power-delay profile (L =3).

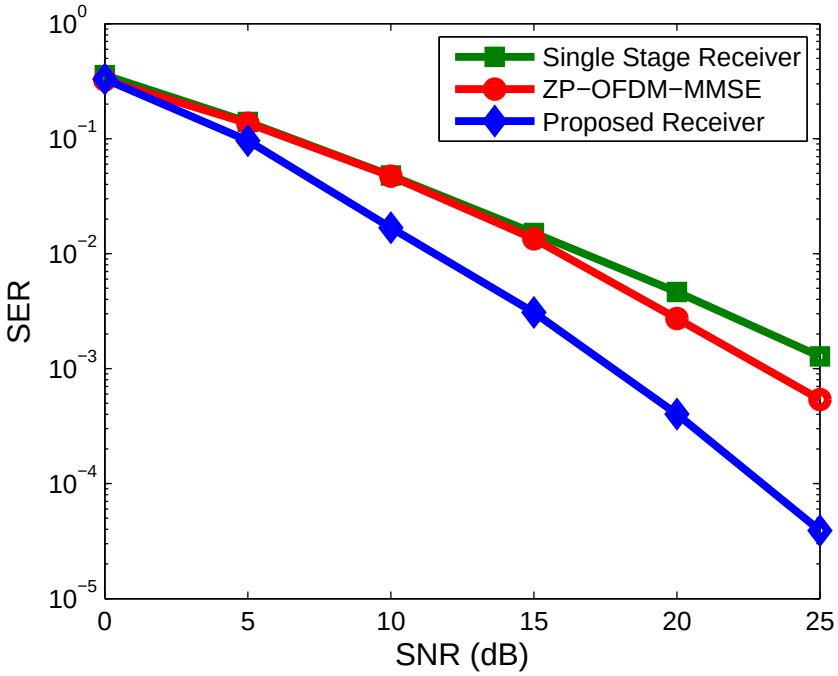

Figure 3.4: BER performance of ZP-OFDM-MMSE, single stage receiver and proposed receiver, uniform power-delay profile (L =4).

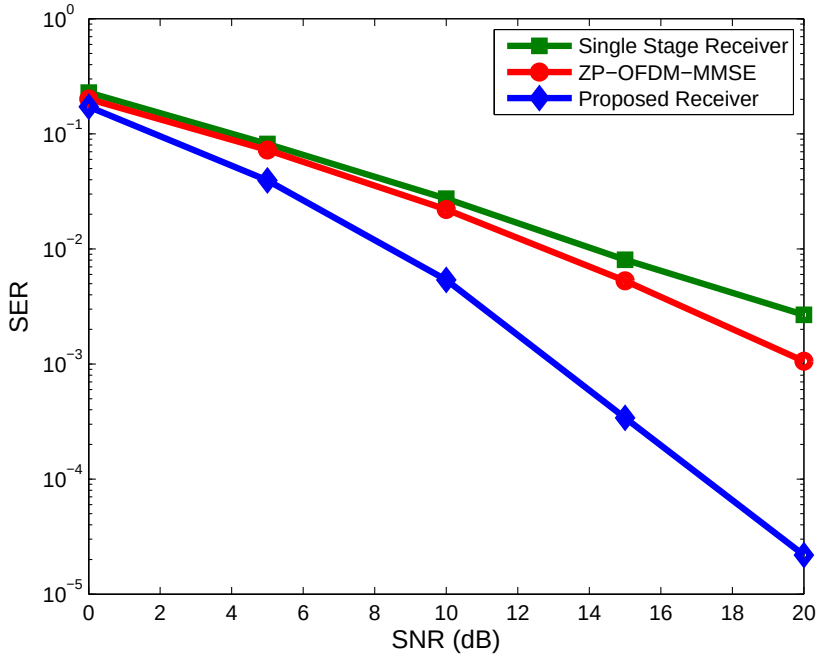

Figure 3.5: BER performance of ZP-OFDM-MMSE, single stage receiver and proposed receiver, exponential power-delay profile (L =6).

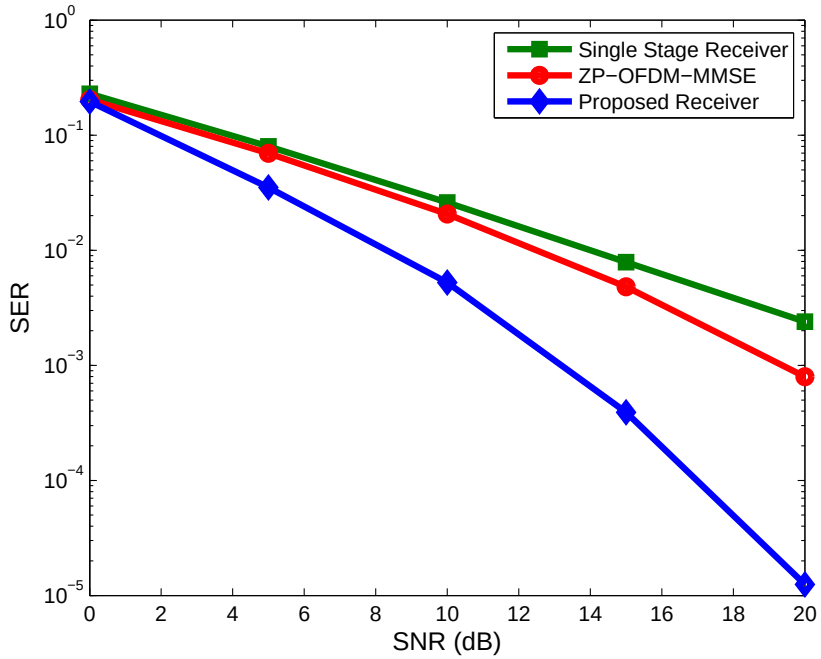

Figure 3.6: BER performance of ZP-OFDM-MMSE, single stage receiver and proposed receiver, exponential power-delay profile (L =7).

Chapter 4

MMSE-Based Receiver Design for Single-Carrier Frequency Domain Equalization

4.1 Introduction

In this chapter, we propose an efficient receiver design for SC-FDE for relay-assisted transmission scenario over frequency selective channels. Building upon our earlier work [5], we propose a novel MMSE-based receiver design tailored to broadband cooperative networks. We show that our MMSE-based receiver is able to collect full antenna and multipath diversity gains. Specifically, under the assumption of perfect power control and high SNR for the underlying links and assuming either of $S \rightarrow R$ or $R \rightarrow D$ links to be frequency selective Rician fading, our performance analysis demonstrates that the proposed receiver is able to achieve a maximum diversity order of $\min(L_{SR}, L_{RD}) + L_{SD} + 2$, where L_{SR}, L_{RD}, and L_{SD} are the channel memory lengths for $S \rightarrow R$, $R \rightarrow D$, and $S \rightarrow D$ links, respectively. Complexity analysis and simulation results demonstrate that our proposed receiver outperforms the conventional cooperative MMSE-SC-FDE receiver by performing close to MFB, while providing minimal computational complexity.

4.2 System Model

A single-relay assisted cooperative communication scenario is considered. All terminals are equipped with single transmit and receive antennas. Any linear modulation technique such as QAM or PSK modulation can be used. We assume AF relaying and adopt the user cooperation protocol proposed by Nabar *et al.* [39]. Specifically, the source terminal communicates with the relay terminal during the first signaling interval. There is no transmission from source-to-destination within this period. In the second signaling interval, both the relay and source terminals communicate with the destination terminal.

The CIRs for $S \rightarrow R$, $S \rightarrow D$ and $R \rightarrow D$ links for the j^{th} transmission block are given by $\mathbf{h}_{SR}^{j} = \left[h_{SR}^{j}[0], ..., h_{SR}^{j}[L_{SR}]\right]^{\mathrm{T}}$, $\mathbf{h}_{RD}^{j} = \left[h_{SD}^{j}[0], ..., h_{SD}^{j}[L_{SD}]\right]^{\mathrm{T}}$ and $\mathbf{h}_{SD}^{j} = \left[h_{RD}^{j}[0], ..., h_{RD}^{j}[L_{RD}]\right]^{\mathrm{T}}$, respectively, where L_{SR}, L_{RD} and L_{SD} denote the corresponding channel memory lengths. The $S \rightarrow R$ link is assumed to be frequency selective Rician fading, while the random vectors $\mathbf{h}_{RD}^{j}$ and $\mathbf{h}_{SD}^{j}$, are assumed to be independent zero-mean complex Gaussian with power delay profile vectors denoted by $\mathbf{v}_{RD} = [\sigma_{RD}^{2}(0), ..., \sigma_{RD}^{2}(L_{RD})]$ and $\mathbf{v}_{SD} = [\sigma_{SD}^{2}(0), ..., \sigma_{SD}^{2}(L_{SD})]$ that are normalized such that $\sum_{l_{RD}=0}^{L_{RD}} \sigma_{RD}^{2}(l_{RD}) = 1$ and $\sum_{l_{SD}=0}^{L_{SD}} \sigma_{SD}^{2}(l_{SD}) = 1$. For the sake of presentation simplicity, the symmetrical scenario, in which the $R \rightarrow D$ link is considered to be frequency selective Rician fading is omitted here. In here we are assuming either of $S \rightarrow R$ or $R \rightarrow D$ to be frequncy selective Rician fading based on the assumption that either of source terminal and relay terminal, or relay terminal and the destination are close enough, so that the LOS path exists. The CIRs are assumed to be constant over two consecutive blocks and vary independently every two blocks.

Information symbols are first parsed to two streams of $M \times 1$ blocks x_{i}^{j}, $i = 1, 2$ and then multiplied by a ZP matrix $\mathbf{\Psi} = \left[\mathbf{I}_{M}^{\mathrm{T}}, \mathbf{0}_{M\times\ell}^{\mathrm{T}}\right]^{\mathrm{T}}$ of size $N \times M$, where $\ell = \max\left(L_{SR}, L_{SD}, L_{RD}\right)$ and N is the frame length. The use of zero-padding as the precoding method in a single-carrier transmission scenario ensures that the available multipath diversity is fully exploited. To further remove inter-block interference and make the channel matrix circulant, a CP with length ℓ is added between adjacent information blocks. Due to the adopted precoding form, i.e., zero padding, we simply insert additional zeros at the start of the frame as CP. The transmitted blocks for $S \rightarrow R$ and $S \rightarrow D$ links are generated by the encoding rule $\mathbf{d}_{1}^{k+1} = -\mathbf{J}\bar{\mathbf{d}}_{2}^{k}$, $\mathbf{d}_{2}^{k+1} = \mathbf{J}\bar{\mathbf{d}}_{1}^{k}$ $k = 0, 2, 4, 6, ...$, where $\mathbf{d}_{i} = \mathbf{\Psi}\mathbf{x}_{i}$, $i = 1, 2$, is the zero-padded information vector and $\mathbf{J} = \mathrm{P}_{N}^{M}$ is a $N \times N$ partial permutation matrix.

4.3 MMSE-based receiver for D-SC-STBC

In this section, we propose a novel, reduced-complexity MMSE-based receiver which enjoys a remarkably simple decoding scheme. We show in the following section that the new proposed receiver is able to collect full antenna and multipath diversity gains, while maintaining minimal complexity.

The proposed receiver includes an MMSE equalizer, followed by linear processing operations. Specifically, the first stage consists of the MMSE-D-STBC-SC scheme [3]. The signal received at the relay terminal during the first signaling interval is

$$\mathbf{r}_R^j = \sqrt{E_{SR}}\mathbf{H}_{SR}^j\mathbf{d}_1^j + \mathbf{n}_R^j, \tag{4.1}$$

where $\mathbf{n}_R^j$ is the additive white Gaussian noise vector with each entry having zero-mean and variance of $N_0/2$ per dimension. The relay terminal normalizes each entry of the received signal $[\mathbf{r}_R^j]_n$, $n = 1, 2, ..., N$, by a factor of $\mathrm{E}\left(|[\mathbf{r}_R^j]_n|^2\right) = E_{SR} + N_0$ to ensure unit average energy and re-transmits the signal during the second time slot. After some mathematical manipulations, the received signal at the destination terminal in the second time slot is given by

$$\mathbf{r}^j = \sqrt{\frac{E_{RD}E_{SR}}{E_{SR}+N_0}}\mathbf{H}_{RD}^j\mathbf{H}_{SR}^j\mathbf{d}_1^j + \sqrt{E_{SD}}\mathbf{H}_{SD}^j\mathbf{d}_2^j + \tilde{\mathbf{n}}^j. \tag{4.2}$$

In (4.2), each entry of the *effective* noise term $\tilde{\mathbf{n}}_j$ (conditioned on $\mathbf{h}_{RD}$) has zero mean and a variance of ρN_0 where ρ is defined by

$$\rho = 1 + \frac{E_{RD}}{E_{SR}+N_0}\sum_{m=0}^{L_3}|\mathbf{h}_{RD}(m)|^2. \tag{4.3}$$

In (4.1)-(4.2), $\mathbf{H}_{SR}^j$, $\mathbf{H}_{SD}^j$ and $\mathbf{H}_{RD}^j$ are $N \times N$ circulant matrices with entries $[\mathbf{H}_i^j]_{k,l} = \mathbf{h}_i^j((k-l) \bmod N)$, i denotes SR, SD, RD, respectively. Finally, E_{SR}, E_{SD} and E_{RD} are the average energies available at the respective terminal which take into account possibly different path loss and shadowing effects between the $S \to D$ and $R \to D$ links, respectively. The destination terminal normalizes the received signal by a factor of $\sqrt{\rho}$. This does not affect the SNR, but simplifies the ensuing presentation [39]. After normalization, we obtain

$$\mathbf{r}^j = \sqrt{\gamma_1}\mathbf{H}_{RD}^j\mathbf{H}_{SR}^j\mathbf{d}_1^j + \sqrt{\gamma_2}\mathbf{H}_{SD}^j\mathbf{d}_2^j + \mathbf{n}^j, \tag{4.4}$$

where $\mathbf{n}^j$ is complex Gaussian with zero mean and variance of $N_0/2$ per dimension and the scaling coefficients γ_1, γ_2 are defined as

$$\gamma_1 = \frac{(E_{SR}/N_0)E_{RD}}{1 + E_{SR}/N_0 + \sum_{m=0}^{L_3} |\mathbf{h}_{RD}(m)|^2 E_{RD}/N_0} \tag{4.5}$$

$$\gamma_2 = \frac{(1 + E_{SR}/N_0)E_{SD}}{1 + E_{SR}/N_0 + \sum_{m=0}^{L_3} |\mathbf{h}_{RD}(m)|^2 E_{RD}/N_0}. \tag{4.6}$$

Assuming that the channel coefficients remain constant over two consecutive blocks, i.e., $\mathbf{H}_i^k = \mathbf{H}_i^{k+1} = \mathbf{H}_i$, i denotes SR, SD, RD, the received signals for blocks j and $j+1$ are given by

$$\mathbf{r}_1{}^j = \sqrt{\gamma_1}\mathbf{H}_{RD}\mathbf{H}_{SR}\mathbf{d}_1^j + \sqrt{\gamma_2}\mathbf{H}_{SD}\mathbf{d}_2^{j+1} + \mathbf{n}^j \tag{4.7}$$

$$\mathbf{r}_2{}^{j+1} = -\sqrt{\gamma_1}\mathbf{H}_{RD}\mathbf{H}_{SR}\mathbf{J}\bar{\mathbf{d}}_2^j + \sqrt{\gamma_2}\mathbf{H}_{SD}\mathbf{J}\bar{\mathbf{d}}_1^{j+1} + \mathbf{n}^{j+1}. \tag{4.8}$$

Next, we transform the received signals to the frequency domain by applying the DFT, i.e., multiplying by the $\mathbf{Q}$ matrix

$$\mathbf{Q}\mathbf{r}^j = \sqrt{\gamma_1}\mathbf{Q}\mathbf{H}_{RD}\mathbf{H}_{SR}\mathbf{d}_1^j + \sqrt{\gamma_2}\mathbf{Q}\mathbf{H}_{SD}\mathbf{d}_2^j + \mathbf{Q}\mathbf{n}^j \tag{4.9}$$

$$\mathbf{Q}\mathbf{J}\bar{\mathbf{r}}^{j+1} = -\sqrt{\gamma_1}\mathbf{Q}\mathbf{H}_{SR}^{\mathrm{H}}\mathbf{H}_{RD}^{\mathrm{H}}\mathbf{d}_2^j + \sqrt{\gamma_2}\mathbf{Q}\mathbf{H}_{SD}^{\mathrm{H}}\mathbf{d}_1^j + \mathbf{Q}\mathbf{J}\bar{\mathbf{n}}^{j+1}. \tag{4.10}$$

Exploiting the circulant structure of the channel matrices, we have

$$\mathbf{H}_i^j = \mathbf{Q}^{\mathrm{H}}\mathbf{\Lambda}_i^j\mathbf{Q}, \tag{4.11}$$

where $\mathbf{\Lambda}_i^j$, i denotes SR, SD, RD, is a diagonal matrix whose (n,n) element is equal to the n^{th} DFT coefficient of $\mathbf{h}_i^j$. Using (4.11) and dropping the subscript j for brevity, we can write (4.9) and (4.10) in matrix form as

$$\begin{bmatrix} \mathbf{Q}\mathbf{r}_1 \\ \mathbf{Q}\mathbf{J}\overline{\mathbf{r}_2} \end{bmatrix} = \begin{bmatrix} \sqrt{\gamma_1}\mathbf{\Lambda}_{RD}\mathbf{\Lambda}_{SR} & \sqrt{\gamma_2}\mathbf{\Lambda}_{SD} \\ \sqrt{\gamma_2}\bar{\mathbf{\Lambda}}_{SD} & -\sqrt{\gamma_1}\bar{\mathbf{\Lambda}}_{RD}\bar{\mathbf{\Lambda}}_{SR} \end{bmatrix} \begin{bmatrix} \mathbf{u}_1^k \\ \mathbf{u}_2^k \end{bmatrix} + \begin{bmatrix} \mathbf{Q}\mathbf{n}^k \\ \mathbf{Q}\mathbf{J}\mathbf{n}^{k+1} \end{bmatrix} = \tilde{\mathbf{\Lambda}}\mathbf{U} + \tilde{\mathbf{N}}, \tag{4.12}$$

where $\mathbf{u}_i^j = \mathbf{Q}\mathbf{d}_i^j$ for $i = 1, 2$ and $j = k, k+1$. Since $\tilde{\mathbf{\Lambda}}$ is an orthogonal matrix of size

$2N \times 2N$, we can multiply (4.12) by

$$\mathbf{K} = \left(\mathbf{I}_2 \otimes \left(\gamma_1 |\mathbf{\Lambda}_{RD}|^2 |\mathbf{\Lambda}_{SR}|^2 + \gamma_2 |\mathbf{\Lambda}_{SD}|^2 \right)^{-1/2} \right) \tilde{\mathbf{\Lambda}}^H. \tag{4.13}$$

The resulting output streams are now decoupled allowing us to write each output sequence as

$$\mathbf{r}_{out,i}^k = \sqrt{\gamma_1 |\mathbf{\Lambda}_{RD}|^2 |\mathbf{\Lambda}_{SR}|^2 + \gamma_2 |\mathbf{\Lambda}_{SD}|^2} \mathbf{Q} \mathbf{d}_i^k + \mathbf{n}_{out,i}^k, \tag{4.14}$$

where $\mathbf{n}_{out,i}^k$ is a noise vector with each entry still Gaussian with zero-mean and variance of $N_0/2$ per dimension. The decoded signal streams in (4.14) are fed into a minimum Euclidean distance decoder yielding $\hat{\mathbf{x}}_1$ and $\hat{\mathbf{x}}_2$, i.e., a decoded version of the transmitted symbols.

$\hat{\mathbf{x}}_1$ and $\hat{\mathbf{x}}_2$, are then fed into the second stage which is capable of exploiting the underlying multipath diversity. Specifically, consider the generation of the matrix $\mathbf{\Pi}_{i,l}$, $l = 0, 1, 2, ..., L$, as follows:

$$[\mathbf{\Pi}_{SRD,l}]_{p,q}, l = 1, ..., L_{SR} + L_{RD} + 1 = \begin{cases} 0 & p - q \bmod N = l \\ [\mathbf{H}_{RD} \mathbf{H}_{SR}]_{p,q} & p - q \bmod N \neq l \end{cases}$$

$$[\mathbf{\Pi}_{SD,l}]_{p,q}, l = 1, ..., L_{SD} + 1 = \begin{cases} 0 & p - q \bmod N = l \\ [\mathbf{H}_{SD}]_{p,q} & p - q \bmod N \neq l \end{cases} \tag{4.15}$$

$$[\mathbf{\Pi}_{SD,l}]_{p,q}, l = L_{SD} + 2, ..., L_{SR} + L_{RD} + 1 = [\mathbf{H}_{SD}]_{p,q},$$

where $1 \leq p, q \leq N$, then, (4.7) and (4.8) can be re-written as

$$\mathbf{y}_1^l = \mathbf{r}_1 - (\sqrt{\gamma_1} \mathbf{\Pi}_{SRD,l} \mathbf{\Psi} \hat{\mathbf{x}}_1 + \sqrt{\gamma_2} \mathbf{\Pi}_{SD,l} \mathbf{\Psi} \hat{\mathbf{x}}_2) \tag{4.16}$$

$$\mathbf{y}_2^l = \mathbf{r}_2 - \left(-\sqrt{\gamma_1} \mathbf{\Pi}_{SRD,l} \mathbf{J} \mathbf{\Psi} \overline{\hat{\mathbf{x}}_2} + \sqrt{\gamma_2} \mathbf{\Pi}_{SD,l} \mathbf{J} \mathbf{\Psi} \overline{\hat{\mathbf{x}}_1} \right). \tag{4.17}$$

Under the high SNR assumption, we can safely assume that $\mathbf{x}_1 \approx \hat{\mathbf{x}}_1$ and $\mathbf{x}_2 \approx \hat{\mathbf{x}}_2$. Therefore, we can write (4.16) and (4.17) as follows:

$$\mathbf{y}_1^l = \sqrt{\gamma_1} \mathbf{H}_{SRD,l} \mathbf{\Psi} \mathbf{x}_1 + \sqrt{\gamma_2} \mathbf{H}_{SD,l} \mathbf{\Psi} \mathbf{x}_2 + \mathbf{n}_1 \tag{4.18}$$

$$\mathbf{y}_2^l = -\sqrt{\gamma_1}\mathbf{H}_{SRD,l}\mathbf{J}\boldsymbol{\Psi}\overline{\hat{\mathbf{x}}_2} + \sqrt{\gamma_2}\mathbf{H}_{SD,l}\mathbf{J}\boldsymbol{\Psi}\overline{\hat{\mathbf{x}}_1} + \mathbf{n}_2, \tag{4.19}$$

where $\mathbf{n}_i$ *(i=1,2)* is complex Gaussian with zero mean and variance of $N_0/2$ per dimension and

$$[\mathbf{H}_{SRD,l}]_{p,q}, \quad l = 1, ..., L_{SR} + L_{RD} + 1 \;\; = \begin{cases} [\mathbf{H}_{RD}\mathbf{H}_{SR}]_{p,q} & p - q \bmod N = l \\ 0 & p - q \bmod N \neq l \end{cases}$$

$$[\mathbf{H}_{SD,l}]_{p,q}, \quad l = 1, ..., L_{SD} + 1 \;\; = \begin{cases} [\mathbf{H}_{SD}]_{p,q} & p - q \bmod N = l \\ 0 & p - q \bmod N \neq l \end{cases} \tag{4.20}$$

$$[\mathbf{H}_{SD,l}]_{p,q}, \quad l = L_{SD} + 2, ..., L_{SR} + L_{RD} + 1 \;\; = 0.$$

Conjugating $\mathbf{J}\mathbf{y}_2^l$ and using the fact $\mathbf{J}\bar{\mathbf{H}}_{i,l}\mathbf{J} = \mathbf{H}_{i,l}^{\mathrm{H}}$, we obtain

$$\mathbf{J}\mathbf{y}_2^l = -\sqrt{\gamma_1}\mathbf{H}_{SRD,l}^{\mathrm{H}}\boldsymbol{\Psi}\mathbf{x}_2 + \sqrt{\gamma_2}\mathbf{H}_{SD,l}^{\mathrm{H}}\boldsymbol{\Psi}\mathbf{x}_1 + \mathbf{J}\bar{\mathbf{n}}_2. \tag{4.21}$$

In matrix form, we can write (4.18) and (4.21) as

$$\begin{bmatrix} \mathbf{y}_1^l \\ \mathbf{J}\bar{\mathbf{y}}_2^l \end{bmatrix} = \underbrace{\begin{bmatrix} \sqrt{\gamma_1}\mathbf{H}_{SRD,l} & \sqrt{\gamma_2}\mathbf{H}_{SD,l} \\ \sqrt{\gamma_2}\mathbf{H}_{SD,l}^{\mathrm{H}} & -\sqrt{\gamma_1}\mathbf{H}_{SRD,l}^{\mathrm{H}} \end{bmatrix}}_{\mathbf{H}_{eq,l}} \begin{bmatrix} \boldsymbol{\Psi}\mathbf{x}_1 \\ \boldsymbol{\Psi}\mathbf{x}_2 \end{bmatrix} + \begin{bmatrix} \mathbf{n}_1 \\ \mathbf{J}\bar{\mathbf{n}}_2 \end{bmatrix}. \tag{4.22}$$

Multiplying (4.22) by

$$\left(\mathbf{I}_2 \otimes \left(\gamma_1|\mathbf{H}_{SRD,l}|^2 + \gamma_2|\mathbf{H}_{SD,l}|^2\right)^{-1/2}\right)\mathbf{H}_{eq,l}^{\mathrm{H}}. \tag{4.23}$$

we observe that the output streams are decoupled (due to orthogonality of $\mathbf{H}_{eq,l}$), allowing us to write

$$\mathbf{z}_i^l = \sqrt{\gamma_1|\mathbf{H}_{SRD,l}|^2 + \gamma_2|\mathbf{H}_{SD,l}|^2}\boldsymbol{\Psi}\mathbf{x}_i + \tilde{\mathbf{n}}_i, \tag{4.24}$$

where the noise term is still complex Gaussian with the variance of $N_0/2$ per dimension. Interestingly, the frequency selective channels are now converted in to parallel independent

frequency flat channels. The signals $\mathbf{z}_i^l, l = 0, 1, ..., L$, can now be combined, resulting in

$$\tilde{\mathbf{z}}_i = \sum_{l=0}^{L} \sqrt{\gamma_1 |\mathbf{H}_{SRD,l}|^2 + \gamma_2 |\mathbf{H}_{SD,l}|^2} \mathbf{\Psi} \mathbf{x}_i + \hat{\mathbf{n}}_i, \tag{4.25}$$

where without loss of generality, $L = L_{SR} + L_{RD} + 1$ and $\hat{\mathbf{n}}_i$ is complex Gaussian with variance of $N_0' = (L+1)N_0/2$ per dimension. The signals in (4.25) are then fed into a maximum likelihood decoder to recover the transmitted symbols.

4.4 Diversity Gain Analysis

Here, we investigate the achievable diversity gain for the proposed receiver through the derivation of the PEP expression.

Defining the transmitted codeword vector and the erroneously-decoded codeword vector as $\mathbf{x}$ and $\hat{\mathbf{x}}$, respectively, and applying the standard Chernoff bound, we obtain

$$P(\mathbf{x}, \hat{\mathbf{x}} | \mathbf{h}_{SR}, \mathbf{h}_{RD}, \mathbf{h}_{SD}) \leq \exp\left(-\frac{d^2(\mathbf{x}, \hat{\mathbf{x}})}{4N'_0}\right), \tag{4.26}$$

where $d^2(\mathbf{x}, \hat{\mathbf{x}})$ denotes the Euclidean distance between $\mathbf{x}$ and $\hat{\mathbf{x}}$. Following [3], the Euclidean distance in (4.26) can be expressed as

$$d^2(\mathbf{x}, \hat{\mathbf{x}}) = \gamma_1 \|\mathbf{H}_{RD}\mathbf{H}_{SR}e_1\|^2 + \gamma_2 \|\mathbf{H}_{SD}e_2\|^2, \tag{4.27}$$

where $\mathbf{e}_i = \mathbf{d}_i - \hat{\mathbf{d}}_i$, $i = 1, 2$.
Having $\|\mathbf{H}_i\|^2 = N \sum_{l_i=0}^{L_i} (|h_i(l_i)|)^2 \quad i = SR, SD$, where N is the frame length, (4.27) can be further simplified to

$$\begin{aligned} d^2(\mathbf{x}, \hat{\mathbf{x}}) &\approx \gamma_1 \textstyle\sum_{l_{RD}=0}^{L_{RD}} \mathbf{h}_{RD}(l_{RD})^2 \|\mathbf{H}_{SR}e_1\|^2 + \gamma_2 \|\mathbf{H}_{SD}e_2\|^2 \\ &\approx \gamma_1 \textstyle\sum_{l_{SR}=0}^{L_{SR}} \mathbf{h}_{SR}(l_{SR})^2 \|\mathbf{H}_{RD}e_1\|^2 + \gamma_2 \|\mathbf{H}_{SD}e_2\|^2 \end{aligned} \tag{4.28}$$

Introducing

$$\Re_i = \begin{bmatrix} [\mathbf{d}]_0 & [\mathbf{d}]_1 & \cdots & [\mathbf{d}]_{N-1} \\ [\mathbf{d}]_{N-1} & [\mathbf{d}]_0 & \cdots & [\mathbf{d}]_{N-2} \\ \vdots & \vdots & \cdots & \vdots \\ [\mathbf{d}]_{N-L_i} & [\mathbf{d}]_{N-L_i+1} & \cdots & [\mathbf{d}]_{N-L_i-1} \end{bmatrix} \tag{4.29}$$

and $\Re_i = (\Re_i - \hat{\Re}_i)(\Re_i - \hat{\Re}_i)^H$, for $i = 1, 2$, (4.28) can be written as follows

$$d^2(\mathbf{x}, \hat{\mathbf{x}}) \approx \gamma_1 \sum_{l_{RD}=0}^{L_{RD}} \mathbf{h}_{RD}(l_{RD})^2 \mathbf{h}_{SR}^T \Re_1 (\mathbf{h}_{SR}^T)^H + \gamma_2 \mathbf{h}_{SD}^T \Re_2 (\mathbf{h}_{SD}^T)^H. \tag{4.30}$$

Defining $\mathbf{\Theta}_i = diag(\mathbf{v}_i)$, $\mu_i = {\mathbf{\Theta}_i}^{-1/2} \mathbf{h}_i$, and $\mathbf{A}_i = \mathbf{\Theta}_i^{1/2} \Re_i \mathbf{\Theta}_i^{1/2}$, $i = SR, SD$, we have

$$d^2(\mathbf{x}, \hat{\mathbf{x}}) \approx \gamma_1 \sum_{l_{RD}=0}^{L_{RD}} \mathbf{h}_{RD}(l_{RD})^2 \mu_{SR}^T \mathbf{A}_{SR} (\mu_{SR}^T)^H + \gamma_2 \mu_{SD}^T \mathbf{A}_{SD} (\mu_{SD}^T)^H, \tag{4.31}$$

where $\mathbf{A}_i$, $i = SR, SD$ are Hermitian and full rank [3]. Therefore, there exists a unitary matrix $\mathbf{U}_{\mathbf{A}_i}$ such that $\mathbf{U}_{\mathbf{A}_i}^H \mathbf{A}_i \mathbf{U}_{\mathbf{A}_i} = \mathbf{\Delta}_i$ where $\mathbf{\Delta}_i$ is a diagonal matrix with elements equal to the eigenvalues of $\mathbf{A}_i$. Therefore, (4.31) can be expressed as

$$d^2(\mathbf{x}, \hat{\mathbf{x}}) \approx \gamma_1 \sum_{l_{RD}=0}^{L_{RD}} \mathbf{h}_{RD}(l_{RD})^2 \beta_{SR} \mathbf{\Delta}_{SR} \beta_{SR}^H + \gamma_2 \beta_{SD} \mathbf{\Delta}_{SD} \beta_{SD}^H, \tag{4.32}$$

where $\beta_i = \mu_i^T \mathbf{U}_{\mathbf{A}_i}$, $i = SR, SD$. Thus, (4.32) can be further simplified to

$$d^2(\mathbf{x}, \hat{\mathbf{x}}) \approx \gamma_1 \sum_{l_{RD}=0}^{L_{RD}} |h_{RD}(l_{RD})|^2 \sum_{l_{SR}=0}^{L_{SR}} \lambda_{SR}(l_{SR}) |\beta_{SR}(l_{SR})|^2 + \gamma_2 \sum_{l_{SD}=0}^{L_{SD}} \lambda_{SD}(l_{SD}) |\beta_{SD}(l_{SD})|^2, \tag{4.33}$$

where $\lambda_{SR}(l_{SR})(\lambda_{SD}(l_{SD}))$ denote the l_{SR}^{th} $\left(l_{SD}^{th}\right)$ eigenvalue of codeword difference matrixes and β_{SR} (β_{SD}) are zero-mean complex Gaussian vectors with unit variance. Assuming perfect power control and sufficiently large $E_{SR}/N_0 > E_{SD}/N_0$ values, the scaling factors in (4.5) and (4.6) reduce to $\gamma_1 = \gamma_2 = E_{SD}$. Then, we can write (6.33) as

$$d^2(\mathbf{x}, \hat{\mathbf{x}}) \approx E_{SD} \sum_{l_{RD}=0}^{L_{RD}} |h_{RD}(l_{RD})|^2 \sum_{l_{SR}=0}^{L_{SR}} \lambda_{SR}(l_{SR}) |\beta_{SR}(l_{SR})|^2 + E_{SD} \sum_{l_{SD}=0}^{L_{SD}} \lambda_{SD}(l_{SD}) |\beta_{SD}(l_{SD})|^2. \tag{4.34}$$

In the following, we will derive the PEP expression under two different scenarios:

Case I: $L_{RD} > L_{SR}$

First, we define the random variables $Y_2 = \sum_{l_{SD}=0}^{L_{SD}} \lambda_{SD}(l_{SD})|\beta_{SD}(l_{SD})|^2$ and $Y_1 = X_1 X_2$ with $X_1 = \sum_{lRD=0}^{L_{RD}} |\mathbf{h}_{RD}(l_{RD})|^2$ and $X_2 = \sum_{l_{SR}=0}^{L_{SR}} \lambda_{SR}(l_{SR})|\beta_{SR}(l_{SR})|^2$. Substituting (4.33) in (4.26) and averaging the resulting expression with respect to Y_1 and Y_2, we obtain

$$\begin{aligned} P(\mathbf{x}, \hat{\mathbf{x}}) &\leq E_{Y_1}\left[\exp\left(-\tfrac{E_{SD}}{4N'_0}Y_1\right)\right] E_{Y_2}\left[\exp\left(-\tfrac{E_{SD}}{4N'_0}Y_2\right)\right] \\ &= \Phi_{Y_1}(\omega)\big|_{j\omega=-\frac{E_{SD}}{4N'_0}} \times \Phi_{Y_2}(\omega)\big|_{j\omega=-\frac{E_{SD}}{4N'_0}}, \end{aligned} \tag{4.35}$$

where $\Phi_{Y_1}(\omega)$ and $\Phi_{Y_2}(\omega)$ are the characteristic functions of Y_1 and Y_2 respectively. Since the entries of $|\beta_{SD}|$ are Rayleigh distributed, $\Phi_{Y_2}(\omega)$ is given as [61]

$$\Phi_{Y_2}(\omega)\big|_{j\omega=-\frac{E_{SD}}{4N'_0}} = \prod_{l_{SD}=0}^{L_{SD}} \left(1 + \frac{E_{SD}}{4N'_0}\lambda_{SD}(l_{SD})\right)^{-1}. \tag{4.36}$$

$\Phi_{Y_1}(\omega)$ can be evaluated as [3]

$$\Phi_{Y1}(\omega) = \int_0^\infty f_{X_1}(x_1)\Phi_{X_2}(\omega x_1)dx_1, \tag{4.37}$$

where $f_{X_1}(x_1)$, $x_1 \geq 0$ is the probability density function (pdf) of X_1, and $\phi_{X_2}(\omega x_1)$ is the characteristic function of X_2. Having X_1 to be a chi squared random variable with $2(L_{RD}+1)$ degrees of freedom [3],

$$f_{X_1}(x_1) = \frac{(L_{RD}+1)^{L_{RD}+1}}{\Gamma(L_{RD}+1)} x_1^{L_{RD}} e^{-(L_{RD}+1)x_1} \tag{4.38}$$

and $\phi_{Y_1}(\omega x_1)$ can be evaluated as [3]

$$\phi_{X_2}(\omega x_1) = \prod_{l_{SR}=0}^{L_{SR}} \left[\frac{1+n^2}{1+n^2-\omega\lambda_{SR}(l_{SR})x_1} e^{\frac{n^2\omega\lambda x_1}{1+n^2-\omega\lambda x_1}}\right]. \tag{4.39}$$

where n is the fading parameter. Having (4.38) and (4.39), (4.37) can be evaluated as

$$\begin{aligned}
&\phi_{Y_1}(\omega)\big|_{j\omega=\frac{-E_{SD}}{4N'_0}} = \\
&= \int_0^\infty \tfrac{(L_{RD}+1)^{L_{RD}+1}}{\Gamma(L_{RD}+1)} x_1^{L_{RD}} e^{-(L_{RD}+1)x_1} \times \textstyle\prod_{l_{SR}=0}^{L_{SR}} \left[\frac{1+n^2}{1+n^2+\frac{E_{SD}}{4N'_0}\lambda_{SR}(l_{SR})x_1} e^{\frac{-n^2\frac{E_{SD}}{4N'_0}\lambda_{SR}(l_{SR})x_1}{1+n^2+\frac{E_{SD}}{4N'_0}\lambda_{SR}(l_{SR})x_1}} \right] \\
&= \tfrac{(L_{RD}+1)^{L_{RD}+1}}{\Gamma(L_{RD}+1)} e^{-(L_{RD}+1)x_1} \quad \times \textstyle\prod_{l_{SR}=0}^{L_{SR}} \int_0^\infty \left[\frac{x_1^{L_{RD}}(1+n^2)}{1+n^2+\frac{E_{SD}}{4N'_0}\lambda_{SR}(l_{SR})x_1} e^{\frac{-n^2\frac{E_{SD}}{4N'_0}\lambda_{SR}(l_{SR})x_1}{1+n^2+\frac{E_{SD}}{4N'_0}\lambda_{SR}(l_{SR})x_1}} \right].
\end{aligned} \tag{4.40}$$

Assuming high SNR, i.e., $E_{SD}/4N'_0 \gg 1$, (4.40) can be simplified as

$$\begin{aligned}
&\phi_{Z_1}(\omega)\big|_{j\omega=\frac{-E_{SD}}{4N'_0}} = R\Big(\tfrac{E_{SD}}{4N'_0}\Big)^{-(L_{SR}+1)} \lambda^{-(L_{SR}+1)} \\
&\times \int_0^\infty \left[\frac{x_1^{L_{RD}}}{\prod_{l_{SR}=0}^{L_{SR}} \frac{1}{\frac{E_{SD}}{4N'_0}\lambda_{SR}(l_{SR})} + \frac{x_1}{1+n^2}} e^{-n^2} e^{-(L_{RD}+1)x_1} \right],
\end{aligned} \tag{4.41}$$

where $R = \frac{(L_{RD}+1)^{L_{RD}+1}}{\Gamma(L_{RD}+1)}$. After further simplification, (4.41) can be written as

$$\phi_{Y_1}(\omega)\big|_{j\omega=\frac{-E_{SD}}{4N'_0}} = \frac{(1+n^2)^{L_{SR}+1}}{(L_{RD}+1)} \frac{e^{-n^2(L_{SR}+1)}}{L_{RD}-L_{SR}} \times R\Big(\frac{E_{SD}}{4N'_0}\Big)^{-(L_{SR}+1)} \lambda^{-(L_{SR}+1)} \Gamma(L_{RD}-L_{SR}). \tag{4.42}$$

Substituting (4.42) and (4.36) in (4.35), we find the final PEP expression given as

$$\begin{aligned}
&P(\mathbf{x},\hat{\mathbf{x}}) \le \tfrac{(1+n^2)^{L_{SR}+1}}{(L_{RD}+1)} \tfrac{e^{-n^2(L_{SR}+1)}}{L_{RD}-L_{SR}} R\Big(\tfrac{E_{SD}}{4N'_0}\Big)^{-(L_{SR}+1)} \\
&\times \lambda^{-(L_{SR}+1)} \Gamma(L_{RD}-L_{SR}) \textstyle\prod_{l_{SD}=0}^{L_{SD}} \Big(1+\tfrac{E_{SD}}{4N'_0}\lambda_{SD}(l_{SD})\Big)^{-1}.
\end{aligned} \tag{4.43}$$

Case II: $L_{SR} > L_{RD}$

Noting that this case is similar to Case I with L_{SR} and L_{RD} interchanged, we consider the random variable $Z_2 = X_2 Y_2$, with $X_2 = \sum_{l_{SR=0}}^{L_{SR}} |h_{SR}(l_{SR})|^2$ and $Y_2 = \sum_{l_{RD=0}}^{L_{RD}} \lambda_{RD}(l_{RD})|h_{RD}(l_{RD})|^2$. The characteristic function of Z_2, ϕ_{Z_2}, can be evaluated as

$$\phi_{Z_2}(\omega) = \int_0^\infty f_{X_2}(u)\phi_{Y_2}(\omega u)du. \tag{4.44}$$

Using the integral form given in [62],

$$f_{X_2}(u) = \left(\frac{(L_{SR}+1+K_R)^{L_{RD}+1}}{1/(L_{SR}+1)}\right)\left[\frac{(L_{SR}+1+K_R)}{K_R(1/(L_{SR}+1))}\right]^{L_{SR}/2} \times e^{-\left[K_R+\frac{(L_{SR}+1+K_R)}{1/(L_{SR}+1)}u\right]} I_{LSR}\left[2\sqrt{\frac{K_R(L_{SR}+1+K_R)}{1/(L_{SR}+1)}u}\right], \tag{4.45}$$

where $K_R = \sum_{l_{SR}=0}^{L_{SR}} K_{l_{SR}}$, and $K_{l_{SR}}$ is the Rician parameter on the ${l_{SR}}^{th}$ tap. (4.44) can be further simplified to

$$\phi_{Z_2}(\omega) = c(\frac{c}{K_R})^{L_{SR}/2} e^{-k_2} \int_0^\infty u^{L_{SR}/2} e^{-cu} I_{L_{SR}}(2\sqrt{K_R c u}) \times \prod_{l_{RD}=0}^{L_{RD}} \frac{1}{1+\frac{E_{SD}}{4N'_0}\lambda_{RD}(l_{RD})u}, \tag{4.46}$$

where $c = (L_{SR}+1+K_R)(L_{SR}+1)$ and $I_{LSR}(\alpha) = \left(\frac{\alpha}{2}\right)^{L_{SR}} \sum_{k=0}^{\infty} \left(\frac{\alpha^2}{4}\right)^k \frac{1}{k!\Gamma(k+L_{SR}+1)}$. Using the fact that $\int_0^\infty y^{n-1}e^{-ay}dy = a^{-u}\Gamma(n)$, after some mathematical manipulations, (4.46) yields

$$\begin{aligned}\phi_{Z_2}(\omega) &= [(L_{SR}+1)(L_{SR}+1+K_R)]^{L_{RD}-L_{SR}/2} \times e^{-K_R}\left(\frac{E_{SD}}{4N'_0}\right)^{-(L_{RD}+1)} \\ &\times \textstyle\prod_{l_{RD}=0}^{L_{RD}} \lambda_{RD}(l_{RD})^{-1} \times \sum_{k=0}^{\infty} K_R \frac{\Gamma(L_{SR}+k-L_{RD})}{k!\Gamma(L_{SR}+k+1)}.\end{aligned} \tag{4.47}$$

Substituting (4.47) and (4.36) in (4.35), we find the final PEP expression given as

$$\begin{aligned}P(\mathbf{x},\hat{\mathbf{x}}) &\le [(L_{SR}+1)(L_{SR}+1+K_R)]^{L_{RD}-L_{SR}/2} \times e^{-K_R}\left(\frac{E_{SD}}{4N'_0}\right)^{-(L_{RD}+1)} \prod_{l_{RD}=0}^{L_{RD}} \lambda_{RD}(l_{RD})^{-1} \\ &\times \sum_{k=0}^{\infty} K_R \frac{\Gamma(L_{SR}+k-L_{RD})}{k!\Gamma(L_{SR}+k+1)} \times \prod_{l_{SD}=0}^{L_{SD}} \left(1+\frac{E_{SD}}{4N'_0}\lambda_{SD}(l_{SD})\right)^{-1}.\end{aligned} \tag{4.48}$$

It is observed from (4.43) and (4.48) that the maximum achievable diversity order is given by $\min(L_{SR}, L_{RD}) + L_{SD} + 2$. This is consistent with the results reported in [3].

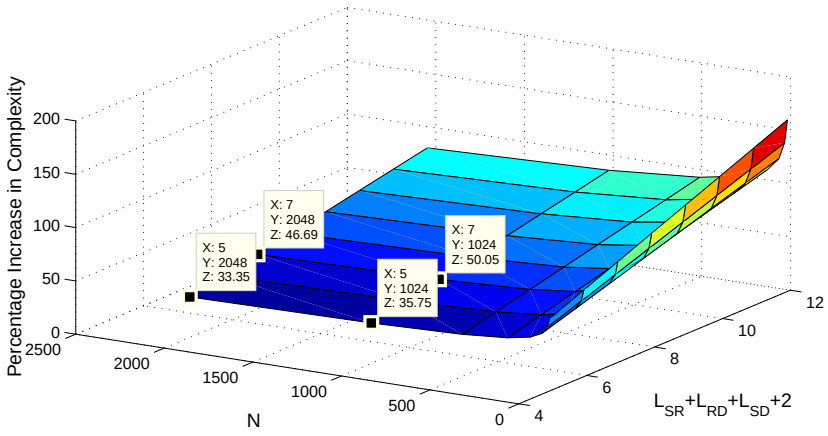

Figure 4.1: Percentage increase in the computational complexity of the proposed receiver compared to MMSE-D-SC-STBC.

4.5 Computational Complexity Analysis

In this section, we focus on the computational complexity of the proposed receiver compared to the conventional MMSE-D-STBC-SC receiver. The computational complexity is measured based on the number of the complex multiplications. The overall computational complexity for the proposed receiver and the conventional MMSE-D-STBC-SC are summarized in Table 4.1. Fig. 4.1 illustrates the percentage increase in the computational complexity of the proposed receiver, plotted against the sum of the memory order of the three links, $L_{SR} + L_{RD} + L_{SD} + 2$, and N. For instance, for $N = 2048$ and $L_{SR} = L_{RD} = L_{SD} = 1$, the computational complexity of the proposed receiver is only 33.3% more compared to the conventional MMSE-D-STBC-SC receiver. This percentage is 37.75% for $N = 1024$ and $L_{SR} = L_{RD} = L_{SD} = 1$ and 46.69% for $N = 2048$ and $L_{SR} + L_{RD} + L_{SD} = 5$, as illustrated in Fig. 4.1. Note that to find the computational complexity of our proposed system, we can also focus on the complexity lying within the calculation of the inverse channel matrix. Focusing on the calculation of inverse channel matrix in (4.13), both our proposed receiver and the conventional MMSE-D-STBC-SC receiver have similar calculation complexity of order $O(N^3)$ [59].

Table 4.1: Comparison of overall computational complexity.

Implementation	Number of Complex Multiplications
MMSE-D-STBC-SC	$N(\log_2^N + 4)$
Proposed	$N(\log_2^N + 4)$ $+(N+1)(L_{SR} + L_{SD} + L_{RD} + 2)$

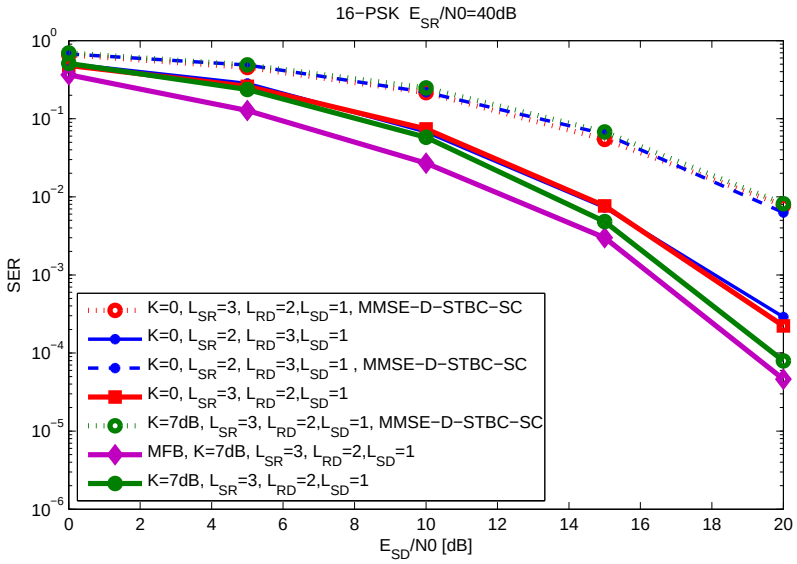

Figure 4.2: SER performance of MMSE-D-STBC-SC and proposed receiver.

4.6 Numerical Results

In this section, we present Monte-Carlo simulation results for the proposed receiver, assuming a quasi-static frequency-selective Rician fading channel for the $S \rightarrow R$ link, which is suitable for suburban areas that a LOS path often exists, and quasi-static Rayleigh fading channels for $S \rightarrow D$ and $R \rightarrow D$ links. We assume 16-PSK modulation. Rician fading is characterized by the $K_{l_{SR}}$ factor ($K_{l_{SR}} = n^2$) which is the power ratio of the LOS and the diffused components. It represents Rayleigh fading for $K_{l_{SR}} = 0$, and no fading when $K_{l_{SR}} \rightarrow \infty$. This makes Rician fading a general model for land mobile channels [63].

First, the scenarios with different combinations of channel memory lengths are studied. We assume $E_{SR}/N_0 = 40$dB and consider three different scenarios:

1) $L_{SR} = 3, L_{RD} = 2, L_{SD} = 1$ and $K = 7$dB

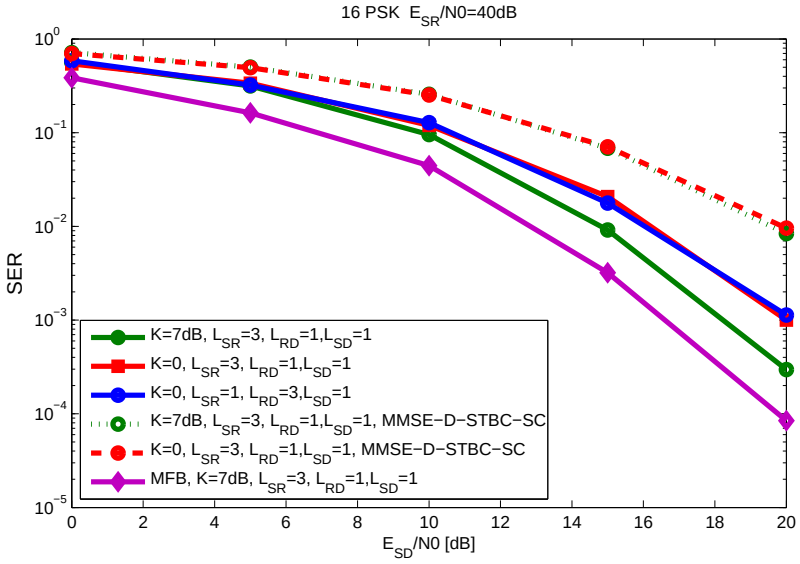

Figure 4.3: SER performance of MMSE-D-STBC-SC and proposed receiver.

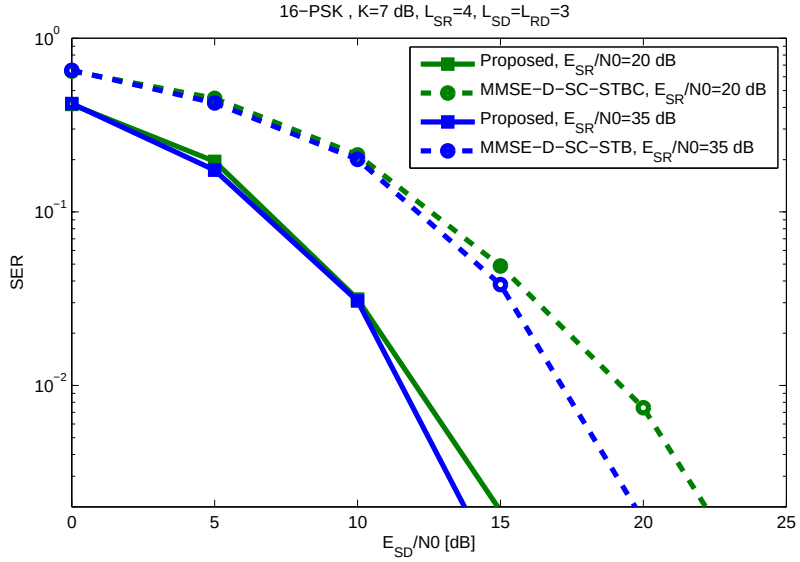

Figure 4.4: SER performance of MMSE-D-STBC-SC and proposed receiver.

2) $L_{SR} = 3, L_{RD} = 2, L_{SD} = 1$ and $K = 0$

3) $L_{SR} = 2, L_{RD} = 3, L_{SD} = 1$ and $K = 0$

Note that we are choosing E_{SR}/N_0= 40dB for the sake of presentation. As long as

$E_{SR}/N_0 \gg 25$dB, its safe to assume that there is no error propagation from the first stage to the feed-back stage.

In Fig. 4.2, Performance of MMSE-D-SC-STBC and the proposed receiver for each of these scenarios is illustrated. As a benchmark, we also include MFB performance, which doesn't take ISI into account. It can be seen that identical SER performance is achieved by interchanging the values of L_{SR} and L_{RD}, which confirms our previous observations from PEP analysis. It is clear from the slope of the curves that our new receiver is able to collect full diversity gains, i.e., $\min(L_{RD}, L_{SR}) + L_{SD} + 2 = 5$, confirming our earlier conclusion. Our simulation results indicate that, for the first scenario, the proposed receiver outperforms the MMSE-D-SC-STBC equalizer by ≈5.5dB at BER $= 10^{-2}$. For the second scenario, the proposed receiver outperforms the MMSE-D-SC-STBC receiver by ≈4.5dB at BER $= 10^{-2}$. The proposed receiver still has a degradation of 1dB compared to the MFB.

Secondly, we assume $E_{SR}/N_0 = 40$dB and consider the following cases in Fig. 4.3, where performance of the following scenarios is analyzed for MMSE-D-SC-STBC and the proposed receiver:

1) $L_{SR} = 3, L_{RD} = 1, L_{SD} = 1$ and K=7dB

2) $L_{SR} = 3, L_{RD} = 1, L_{SD} = 1$ and K=0dB

3) $L_{SR} = 1, L_{RD} = 3, L_{SD} = 1$ and K=0dB

4) $L_{SR} = 1, L_{RD} = 3, L_{SD} = 1$ and K=7dB

Note that similar SER performance is acheived while interchanging the values of L_{SR} and L_{RD}. Our results indicate that for the first scenario, the proposed receiver outperforms the MMSE-D-SC-STBC equalizer by 4.5dB at BER $= 10^{-2}$. Having $L_{SR} + L_{RD} + L_{SD} + 2 = 7$, the number of complex multiplications for the proposed receiver is 1095 while the MMSE-D-STBC-SC receiver employs 640 complex multiplication. This extra cost gives ≈4.5dB performance increase at SER $= 10^{-2}$ for the proposed receiver. For the second scenario, the proposed receiver outperforms the MMSE-D-SC-STBC receiver by ≈3dB at BER $= 10^{-2}$. The proposed receiver has a degradation of 2dB compared to the MFB.

In Fig. 4.4, we assume $L_{SR} = 4, L_{RD} = L_{SD} = 3$ and K=7dB and study the performance of the system for different E_{SR}/N_0 values. The performance of the proposed receiver degrades as E_{SR}/N_0 decreases, which confirms our earlier observations. It can be

seen that at SER $= 10^{-2}$, the proposed receiver working at E_{SR}/N_0=35dB outperforms its counterpart working at E_{SR}/N_0=5dB by 15dB. Interestingly, it is observed from Figs. 4.2, 4.3 and 4.4 that performance improvement of the proposed receiver, in comparison to the benchmark, increases as L increases, which comes at low additional cost.

4.7 Summary

We propose a novel reduced-complexity MMSE-based receiver for D-SC-STBC transmissions. We show that our MMSE-based receiver is able to collect full antenna and multipath diversity gains. We show that the computational complexity of our proposed system is comparable to the conventional MMSE-D-SC-STBC receiver while collecting the maximum achievable diversity order of $\min(L_{SR}, L_{RD}) + L_{SD} + 2$. Simulation results demonstrate that our proposed receiver outperforms the conventional MMSE-D-SC-STBC receiver, while maintaining low complexity tradeoff.

Chapter 5

Distributed Single-Carrier Frequency Domain Equalization in Multi-Relay Networks.

5.1 introduction

In this chapter, we investigate the performance of SC-FDE for D-STBC systems with AF relaying over frequency-selective Rician fading channels. Our performance analysis demonstrates that SC-FDE for DSTB is able to achieve a maximum diversity order of $\sum_{i=1}^{R} \min(L_{SR_i}, L_{R_iD}) + R$, where R is the number of participating relays, L_{SR_i} and L_{R_iD} are the channel memory lengths for source to i^{th} relay ($S \rightarrow R_i$) link and i^{th} relay to destination ($R_i \rightarrow D$) link, respectively. Simulation results are provided to corroborate the theoretical analysis.

5.2 overview

A combination of STBC with SC-FDE for frequency-selective channels was presented in [64]. Most of the current literature on SC-FDE is limited to point-to-point communication systems. However, there have been recent results reported on FDE in the context of cooperative scenarios [3, 4]. Assuming the MLSD equalizers, D-STBC SC-FDE has been first discussed in [3] as an extension of conventional STBC to cooperative systems. The results

in [3], however, are restricted to a single-relay scenario with AF relaying over Rayleigh fading channels. The asymptotical PEP behavior for a large number of relays is analyzed in [65, 66], but this analysis is restricted to frequency flat Rayleigh fading channels.

In this chapter, we extend the work in [3] to a multi-relay scenario. In particular, we drive a PEP expression for D-SC-FDE-STBC over frequency-selective Rician fading channels and show that the maximum achievable diversity order is $\sum_{i=1}^{R} \min(L_{SR_i}, L_{R_iD}) + R$.

5.3 Transmission Model

We consider a multiple-relay assisted cooperative wireless communication system with a single source (S), R half-duplex relay terminals (R_i), $i = 1, 2, ..., R$, and a single destination (D). The source, destination, and all relays are equipped with single transmit and receive antennas. Any linear modulation technique such as QAM or PSK can be used. We adopt the transmission protocol in [65] and consider AF relaying. Note that unlike [65], we assume that there is no direct transmission between the source and destination terminals due to the presence of shadowing.

The CIRs for $S \rightarrow R_i$ and $R_i \rightarrow D$ links for the i^{th} relay terminal are given by $\mathbf{h}_{SR_i} = \left[h_{SR_i}[0], ..., h_{SR}[L_{SR_i}]\right]^{\mathrm{T}}$, $\mathbf{h}_{R_iD} = \left[h_{R_iD}[0], ..., h_{R_iD}[L_{R_iD}]\right]^{\mathrm{T}}$, respectively, where L_{SR_i} and L_{R_iD} denote the corresponding channel memory lengths. All the $S \rightarrow R_i$ and $R_i \rightarrow D$ links are assumed to be frequency selective Rician fading. The random vectors $\mathbf{h}_{SR_i}$ and $\mathbf{h}_{R_iD}$ are assumed to be independent zero-mean complex Gaussian with power delay profile vectors denoted by $\mathbf{v}_{SR_i} = [\sigma^2_{SR_i}(0), ..., \sigma^2_{SR_i}(L_{SR_i})]$ and $\mathbf{v}_{R_iD} = [\sigma^2_{R_iD}(0), ..., \sigma^2_{R_iD}(L_{R_iD})]$ that are normalized such that $\sum_{l_{SR_i}=0}^{L_{SR_i}} \sigma^2_{SR_i}(l_{SR_i}) = 1$ and $\sum_{l_{R_iD}=0}^{L_{R_iD}} \sigma^2_{R_iD}(l_{R_iD}) = 1$. The CIRs are assumed to be constant over eight consecutive blocks and vary independently every eight blocks, where each block consists of five time slots. In the following, we will briefly review space-time block codes, where this knowledge is fundamental to the rest of this chapter.

The $p \times n$ space-time block code transmission matrix $\mathcal{G}$, contains entries that are linear combinations of the variables $x_1, x_2, ..., x_M$ and their conjugates. The complex space-time block code $\mathcal{C}$ can be constructed, with its entries c_{ti}, being $\pm x_1, \pm x_2, ..., \pm x_M$, their conjugates, or their multiples [16]. Having c_{ti} to be the element in the t^{th} row and i^{th} column of matrix $\mathcal{C}$, at each time slot $t = 1, 2, ..., p$, c_{ti} are transmitted simultaneously from antennas $i = 1, 2, ..., n$. Note that in our choice of design, the source terminal is equipped with a single antenna and the parameter n, will therefore, be replaced with the number of relays

R. So, the i^{th} column of matrix $\mathcal{C}$ represents the information symbol transmitted to the i^{th} relay R_i and the t^{th} row of matrix $\mathcal{C}$ represents the information symbols transmitted at time slot t. Having matrix $\mathcal{C}$ built upon $\mathcal{G}$, and using the orthogonality between $\mathcal{G}$'s columns, we are able to use a simple decoding scheme [20]. Note that since $R \cdot p$ time slots are used to send M information symbols, the rate $R_{\mathcal{C}}$ of the space-time code $\mathcal{C}$ can be defined as $R_{\mathcal{C}} = \frac{M}{Rp}$. As an example, the $\mathcal{G}_2$ code has rate one.

In the following, we consider the rate $\frac{1}{2}$ space-time block code $\mathcal{G}_4$[20] with four relays in a cooperative scenario with AF relaying. We would like to point out that extension to a multiple relay scenario is straightforward. Note that since $\mathcal{G}_4$ can be decomposed into $\mathcal{G}_4 = \begin{pmatrix} \mathcal{G}_d \\ conj(\mathcal{G}_d) \end{pmatrix}$, we can divide the encoding process into two sections, each targeting half of the entries in $\mathcal{G}_4$.

Information symbols are first parsed as four streams of $M \times 1$ blocks x_i, $i = 1, 2, 3, 4$ and encoded to $\mathbf{c}_{ti}$ using the orthogonal space-time block code design $\mathcal{C}$. They are further multiplied by a ZP matrix $\mathbf{\Psi} = \left[\mathbf{I}_M^{\mathrm{T}}, \mathbf{0}_{M\times\ell_i}^{\mathrm{T}}\right]^{\mathrm{T}}$ of size $N \times M$, where $\ell_i = \max\left(L_{SR_i}, L_{R_iD}\right)$ and N is the frame length. Note that zero-padding is a precoding method used in single-carrier transmissions to ensure that the available multipath diversity is fully exploited. To further remove the inter-block interference and make the channel matrix circulant, a CP with length ℓ_i is added between adjacent information blocks. Due to the adopted precoding form, i.e., zero padding, additional zeros are inserted at the start of the frame as CP.

During every five time slots, four time slots are devoted to signal transmission from source to relays, one at a time, and during the last time slot, all R relays retransmit the normalized received signals to the destination terminal. The signal received at i^{th}, $(i = 1, 2, 3, 4)$, relay terminal during time slot t is

$$\mathbf{r}_{R_i}^t = \sqrt{E_{SR_i}}\mathbf{H}_{SR_i}\mathbf{d}_i^r + \mathbf{n}_{R_i}, \tag{5.1}$$

where r is the row number in the $\mathcal{G}$ code, i.e., $r = 1, 2, ..., 8$ in the $\mathcal{G}_4$ code, $t = i + 5r - 5$, $\mathbf{d}_i^r = \mathbf{\Psi}\mathbf{c}_{ri}$ is the zero-padded information vector, and $\mathbf{n}_{R_i}$ is the additive white Gaussian noise vector with each entry having zero-mean and variance of $N_0/2$ per dimension. To ensure unit average energy [4], each relay terminal normalizes each entry of the received signal $[\mathbf{r}_{R_i}^t]_n$, $n = 1, 2, ..., N$, by a factor of $\mathrm{E}\left(\left|[\mathbf{r}_{R_i}^t]_n\right|^2\right) = E_{SR_i} + N_0$ and re-transmits the signal during the fifth time slot as

$$\mathbf{r}_{R_i}^t = \sqrt{\frac{E_{SR_i}}{E_{SR_i}+N_0}}\mathbf{H}_{SR_i}\mathbf{d}_i^r + \frac{\mathbf{n}_{R_i}}{\sqrt{E_{SR_i}+N_0}}. \tag{5.2}$$

In (5.1)-(5.2), $\mathbf{H}_{SR_i}$ is an $N \times N$ circulant matrices with entries $[\mathbf{H}_{SR_i}]_{k,l} = \mathbf{h}_{SR_i}((k-l) \bmod N)$, and E_{SR_i} is the average energy available at relay. During the last signaling interval of every five time slots, all the four relays retransmit the normalized received signal to the destination terminal, and the destination receives (5.3)

$$\mathbf{r}_D^{5r} = \sum_{t=5r-4}^{5r-1} \mathbf{r}_{R_i}^t = \sum_{i=1}^{4} \sqrt{\frac{E_{R_iD}E_{SR_i}}{E_{SR_i}+N_0}}\mathbf{H}_{R_iD}\mathbf{H}_{SR_i}\mathbf{d}_i^r + \tilde{\mathbf{n}}_D^t, \tag{5.3}$$

where $r = 1, 2, 3, 4$, and each entry of the *effective* noise term $\tilde{\mathbf{n}}_D^t$ (conditioned on $\mathbf{h}_{R_iD}$) has zero mean and a variance of ρN_0 where ρ is defined by

$$\rho = 1 + \sum_{i=1}^{R} \frac{E_{R_iD}}{E_{SR_i}+N_0} \sum_{l=0}^{L_{R_iD}} |\mathbf{h}_{R_iD}(l)|^2. \tag{5.4}$$

The destination terminal normalizes the received signal in (5.3) by a factor of $\sqrt{\rho}$. This does not affect the SNR, but simplifies the ensuing presentation [3, 67]. After normalization, we obtain

$$\mathbf{r}_D^{5r} = \sum_{i=1}^{4} \sqrt{\gamma_i}\mathbf{H}_{R_iD}\mathbf{H}_{SR_i}\mathbf{d}_i^r + \hat{\mathbf{n}}_D^t, r = 1, 2, 3, 4 \tag{5.5}$$

where $\hat{\mathbf{n}}_D^t$ is complex Gaussian with zero mean and variance of $N_0/2$ per dimension and the scaling coefficients γ_i is defined as

$$\gamma_i = \frac{E_{R_iD}E_{SR_i}}{E_{SR_i}+N_0\left(1+\sum_{i=1}^{R}\frac{E_{R_iD}}{E_{SR_i}+N_0}\sum_{l=0}^{L_{R_iD}}\left|\mathbf{h}_{R_iD}(l)\right|^2\right)} = \frac{\prod_{j=1}^{R}(1+SNR_{SR_{j\neq i}})SNR_{R_iD}E_{SR_i}}{\prod_{j=1}^{R}(1+SNR_{SR_j})+\sum_{i=1}^{R}\left(\prod_{j=1}^{R}(1+SNR_{SR_{j\neq i}})\right)SNR_{R_iD}\sum_{l=0}^{L_{R_iD}}\left|\mathbf{h}_{R_iD}(l)\right|^2}, \tag{5.6}$$

where $SNR_{SR_j} = \frac{E_{SR_j}}{N_0}$, and $SNR_{R_iD} = \frac{E_{R_iD}}{N_0}$. During the next twenty time slots which covers the second half of space-time block code $\mathcal{G}_4$, we will be following similar encoding rule, except that the transmitted blocks are processed with the $\mathbf{J} = \mathrm{P}_N^M$, which is an $N \times N$

partial permutation matrix. Assuming that the channel coefficients remain constant over eight consecutive blocks, the received signals for blocks 1 to 8 are given by

$$\mathbf{r}_D^5 = \sqrt{\gamma_1}\mathbf{H}_{R_1D}\mathbf{H}_{SR_1}\tilde{\mathbf{d}}_1 + \sqrt{\gamma_2}\mathbf{H}_{R_2D}\mathbf{H}_{SR_2}\tilde{\mathbf{d}}_2 + \sqrt{\gamma_1}\mathbf{H}_{R_3D}\mathbf{H}_{SR_3}\tilde{\mathbf{d}}_3 + \sqrt{\gamma_1}\mathbf{H}_{R_4D}\mathbf{H}_{SR_4}\tilde{\mathbf{d}}_4 + \hat{\mathbf{n}}_D^5, \tag{5.7}$$

$$\mathbf{r}_D^{10} = -\sqrt{\gamma_1}\mathbf{H}_{R_1D}\mathbf{H}_{SR_1}\tilde{\mathbf{d}}_2 + \sqrt{\gamma_2}\mathbf{H}_{R_2D}\mathbf{H}_{SR_2}\tilde{\mathbf{d}}_1 - \sqrt{\gamma_1}\mathbf{H}_{R_3D}\mathbf{H}_{SR_3}\tilde{\mathbf{d}}_4 + \sqrt{\gamma_1}\mathbf{H}_{R_4D}\mathbf{H}_{SR_4}\tilde{\mathbf{d}}_3 + \hat{\mathbf{n}}_D^{10}, \tag{5.8}$$

$$\mathbf{r}_D^{15} = -\sqrt{\gamma_1}\mathbf{H}_{R_1D}\mathbf{H}_{SR_1}\tilde{\mathbf{d}}_3 + \sqrt{\gamma_2}\mathbf{H}_{R_2D}\mathbf{H}_{SR_2}\tilde{\mathbf{d}}_4 + \sqrt{\gamma_1}\mathbf{H}_{R_3D}\mathbf{H}_{SR_3}\tilde{\mathbf{d}}_1 - \sqrt{\gamma_1}\mathbf{H}_{R_4D}\mathbf{H}_{SR_4}\tilde{\mathbf{d}}_2 + \hat{\mathbf{n}}_D^{15}, \tag{5.9}$$

$$\mathbf{r}_D^{20} = -\sqrt{\gamma_1}\mathbf{H}_{R_1D}\mathbf{H}_{SR_1}\tilde{\mathbf{d}}_4 - \sqrt{\gamma_2}\mathbf{H}_{R_2D}\mathbf{H}_{SR_2}\tilde{\mathbf{d}}_3 + \sqrt{\gamma_1}\mathbf{H}_{R_3D}\mathbf{H}_{SR_3}\tilde{\mathbf{d}}_2 + \sqrt{\gamma_1}\mathbf{H}_{R_4D}\mathbf{H}_{SR_4}\tilde{\mathbf{d}}_1 + \hat{\mathbf{n}}_D^{20}. \tag{5.10}$$

$\mathbf{r}_D^{25}, \mathbf{r}_D^{30}, \mathbf{r}_D^{35}$ and $\mathbf{r}_D^{40}$ are generated similar to (5.7), (5.8), (5.9) and (5.10), respectively, except that $\tilde{\mathbf{d}}_i$ is replaced with $\bar{\tilde{\mathbf{d}}}_i$, where $\tilde{\mathbf{d}}_i = \mathbf{\Psi}\mathbf{x}_i$, $i = 1, 2, 3, 4$. Next, we transform the received signals to the frequency domain by applying the DFT, i.e., multiplying by the $\mathbf{Q}$ matrix. As an example, $\mathbf{r}_D^5$ and $\mathbf{r}_D^{25}$ are transformed to

$$\begin{aligned}\mathbf{Q}\mathbf{r}_D^5 &= \sqrt{\gamma_1}\mathbf{Q}\mathbf{H}_{R_1D}\mathbf{H}_{SR_1}\tilde{\mathbf{d}}_1 + \sqrt{\gamma_2}\mathbf{Q}\mathbf{H}_{R_2D}\mathbf{H}_{SR_2}\tilde{\mathbf{d}}_2 \\ &+\sqrt{\gamma_1}\mathbf{Q}\mathbf{H}_{R_3D}\mathbf{H}_{SR_3}\tilde{\mathbf{d}}_3 + \sqrt{\gamma_1}\mathbf{Q}\mathbf{H}_{R_4D}\mathbf{H}_{SR_4}\tilde{\mathbf{d}}_4 + \mathbf{Q}\hat{\mathbf{n}}_D^5,\end{aligned} \tag{5.11}$$

$$\begin{aligned}\mathbf{Q}\mathbf{J}\bar{\mathbf{r}}_D^{25} &= \sqrt{\gamma_1}\mathbf{Q}\mathbf{H}_{R_1D}^H\mathbf{H}_{SR_1}^H\mathbf{J}\tilde{\mathbf{d}}_1 + \sqrt{\gamma_2}\mathbf{H}_{R_2D}\mathbf{H}_{SR_2}\bar{\mathbf{J}}\mathbf{d}_2 \\ &+\sqrt{\gamma_1}\mathbf{H}_{R_3D}\mathbf{H}_{SR_3}\bar{\mathbf{J}}\mathbf{d}_3 + \sqrt{\gamma_1}\mathbf{H}_{R_4D}\mathbf{H}_{SR_4}\bar{\mathbf{J}}\mathbf{d}_4 + \mathbf{Q}\bar{\mathbf{J}}\mathbf{n}_D^{25}.\end{aligned} \tag{5.12}$$

Exploiting the circulant structure of the channel matrices, we have

$$\mathbf{H}_{SR_i} = \mathbf{Q}^{\mathrm{H}}\mathbf{\Lambda}_{SR_i}\mathbf{Q}, \tag{5.13}$$

$$\mathbf{H}_{R_iD} = \mathbf{Q}^{\mathrm{H}}\mathbf{\Lambda}_{R_iD}\mathbf{Q}, \tag{5.14}$$

where $\mathbf{\Lambda}_{SR_i}$ and $\mathbf{\Lambda}_{R_iD}$ are diagonal matrices whose (n, n) element is equal to the n^{th} DFT coefficient of $\mathbf{h}_{SR_i}$ and $\mathbf{h}_{R_iD}$, respectively. As an example, (5.11) and (5.12) can be rewritten in the following format

$$\begin{aligned}\mathbf{Q}\mathbf{r}_D^5 &= \sqrt{\gamma_1}\Lambda_{R_1D}\Lambda_{SR_1}\mathbf{Q}\tilde{\mathbf{d}}_1 + \sqrt{\gamma_2}\Lambda_{R_2D}\Lambda_{SR_2}\mathbf{Q}\tilde{\mathbf{d}}_2 \\ &+\sqrt{\gamma_1}\Lambda_{R_3D}\Lambda_{SR_3}\mathbf{Q}\tilde{\mathbf{d}}_3 + \sqrt{\gamma_1}\Lambda_{R_4D}\Lambda_{SR_4}\mathbf{Q}\tilde{\mathbf{d}}_4 + \mathbf{Q}\hat{\mathbf{n}}_D^5,\end{aligned} \tag{5.15}$$

$$\begin{aligned}\mathbf{QJ}\bar{\mathbf{r}}_D^{25} &= \sqrt{\gamma_1}\bar{\Lambda}_{R_1D}\bar{\Lambda}_{SR_1}\mathbf{QJ}\tilde{\mathbf{d}}_1 + \sqrt{\gamma_2}\bar{\Lambda}_{R_2D}\bar{\Lambda}_{SR_2}\mathbf{QJ}\bar{\mathbf{d}}_2 \\ &+\sqrt{\gamma_1}\bar{\Lambda}_{R_3D}\bar{\Lambda}_{SR_3}\mathbf{QJ}\bar{\mathbf{d}}_3 + \sqrt{\gamma_1}\bar{\Lambda}_{R_4D}\bar{\Lambda}_{SR_4}\mathbf{QJ}\bar{\mathbf{d}}_4 + \mathbf{QJ}\bar{\mathbf{n}}_D^{25}.\end{aligned} \tag{5.16}$$

Therefore, we can have the following matrix presentation

$$\begin{bmatrix} \mathbf{Q}\mathbf{r}_D^5 \\ \vdots \\ \mathbf{QJ}\bar{\mathbf{r}}_D^{40} \end{bmatrix} = \begin{bmatrix} \sqrt{\gamma_3}\Lambda_{R_3D}\Lambda_{SR_3} & \cdots & \sqrt{\gamma_2}\Lambda_{R_2D}\Lambda_{SR_2} \\ \vdots & \cdots & \vdots \\ \sqrt{\gamma_4}\bar{\Lambda}_{R_4D}\bar{\Lambda}_{SR_4} & \cdots & -\sqrt{\gamma_1}\bar{\Lambda}_{R_1D}\bar{\Lambda}_{SR_1} \end{bmatrix} \begin{bmatrix} \mathbf{u}_1 \\ \vdots \\ \mathbf{u}_4 \end{bmatrix} + \begin{bmatrix} \mathbf{Q}\hat{\mathbf{n}}_D^5 \\ \vdots \\ \mathbf{QJ}\bar{\mathbf{n}}_D^{40} \end{bmatrix} = \tilde{\Lambda}\mathbf{U} + \tilde{\mathbf{N}}, \tag{5.17}$$

where $\mathbf{u}_i = \mathbf{Q}\tilde{\mathbf{d}}_i$, for $i = 1, 2, 3, 4$. Since $\tilde{\mathbf{\Lambda}}$ is an orthogonal matrix of size $8N \times 8N$, we can multiply (5.17) (without loss of optimality) by

$$\mathbf{K} = \left(\mathbf{I}_4 \otimes \left(\sum_{i=1}^{4} \gamma_i |\mathbf{\Lambda}_{R_iD}|^2 |\mathbf{\Lambda}_{SR_i}|^2 \right)^{-1/2} \right) \tilde{\mathbf{\Lambda}}^H. \tag{5.18}$$

The resulting output streams are now decoupled allowing us to write each output sequence as

$$\mathbf{r}_{out,i} = \sqrt{\sum_{j=1}^{4} \gamma_j \left|\mathbf{\Lambda}_{R_jD}\right|^2 \left|\mathbf{\Lambda}_{SR_j}\right|^2} \mathbf{Q}\tilde{\mathbf{d}}_i + \mathbf{n}_{out,i}, \tag{5.19}$$

where $\mathbf{n}_{out,i}$ is a noise vector with each entry still Gaussian with zero-mean and variance of $N_0/2$ per dimension. The result in (5.19) can be further generalized to the scenario with R relays as follows

$$\mathbf{r}_{out,i} = \sqrt{\sum_{j=1}^{R} \gamma_j \left|\mathbf{\Lambda}_{R_jD}\right|^2 \left|\mathbf{\Lambda}_{SR_j}\right|^2} \mathbf{Q}\tilde{\mathbf{d}}_i + \mathbf{n}_{out,i}. \tag{5.20}$$

The decoded signal streams in (5.20) are fed into an equalizer, yielding $\hat{\mathbf{x}}_1$, $\hat{\mathbf{x}}_\mathbf{2}$, , and $\hat{\mathbf{x}}_M$, i.e., a decoded version of the transmitted symbols.

5.4 Diversity Gain Analysis

In this section, the achievable diversity gain for the multiple relay D-SC-STBC system is investigated, through the derivation of the PEP expression. Defining the transmitted codeword vector and the erroneously-decoded codeword vector as $\mathbf{x}$ and $\hat{\mathbf{x}}$, respectively, the

conditional PEP is given as

$$P(\mathbf{x}, \hat{\mathbf{x}}, \mathbf{h}_{SR_1}, \mathbf{h}_{R_1D}, ..., \mathbf{h}_{SR_R}, \mathbf{h}_{R_RD}) = Q\left(\sqrt{\frac{d^2(\mathbf{x}, \hat{\mathbf{x}})}{2N_0}}\right), \tag{5.21}$$

where $Q(.)$ is the Gaussian-Q function and $d^2(\mathbf{x}, \hat{\mathbf{x}})$ denotes the Euclidean distance between $\mathbf{x}$ and $\hat{\mathbf{x}}$. Applying the standard Chernoff bound to (5.21), we obtain,

$$P(\mathbf{x}, \hat{\mathbf{x}} | \mathbf{h}_{SR_1}, \mathbf{h}_{R_1D}, ..., \mathbf{h}_{SR_R}, \mathbf{h}_{R_RD}) \leq \exp\left(-\frac{d^2(\mathbf{x}, \hat{\mathbf{x}})}{4N_0}\right). \tag{5.22}$$

Following similar steps detailed in [3], the Euclidean distance in (5.22) can be expressed as

$$d^2(\mathbf{x}, \hat{\mathbf{x}}) = \gamma_1 \|\mathbf{H}_{R_1D}\mathbf{H}_{SR_1}e_1\|^2 + \gamma_2 \|\mathbf{H}_{R_2D}\mathbf{H}_{SR_2}e_2\|^2 + ... + \gamma_R \|\mathbf{H}_{R_RD}\mathbf{H}_{SR_R}e_R\|^2, \tag{5.23}$$

where $\mathbf{e}_i = \tilde{\mathbf{d}}_i - \hat{\tilde{\mathbf{d}}}_i$, $i = 1, 2, ..., R$. Having $\|\mathbf{H}_{SR_i}\|^2 = N \sum_{l_i=0}^{L_{SR_i}} (|h_{SR_i}(l_i)|)^2$ and $\|\mathbf{H}_{R_iD}\|^2 = N \sum_{l_i=0}^{L_{R_iD}} (|h_{R_iD}(l_i)|)^2$, (5.23) can be further simplified to

$$d^2(\mathbf{x}, \hat{\mathbf{x}}) \approx \sum_{i=1}^{R} \gamma_i \sum_{l_{R_iD=0}}^{L_{R_iD}} \mathbf{h}_{R_iD}(l_{R_iD})^2 \|\mathbf{H}_{SR_i}e_i\|^2 \approx \sum_{i=1}^{R} \gamma_i \sum_{l_{SR_i=0}}^{L_{SR_i}} \mathbf{h}_{SR_i}(l_{SR_i})^2 \|\mathbf{H}_{R_iD}e_i\|^2. \tag{5.24}$$

Introducing

$$\Re_i = \begin{bmatrix} [\tilde{\mathbf{d}}]_0 & [\tilde{\mathbf{d}}]_1 & \cdots & [\tilde{\mathbf{d}}]_{N-1} \\ [\tilde{\mathbf{d}}]_{N-1} & [\tilde{\mathbf{d}}]_0 & \cdots & [\tilde{\mathbf{d}}]_{N-2} \\ \vdots & \vdots & \cdots & \vdots \\ [\tilde{\mathbf{d}}]_{N-L_{SR_i}} & [\tilde{\mathbf{d}}]_{N-L_{SR_i}+1} & \cdots & [\tilde{\mathbf{d}}]_{N-L_{SR_i}-1} \end{bmatrix} \tag{5.25}$$

and $\Re_i = (\Re_i - \hat{\Re}_i)(\Re_i - \hat{\Re}_i)^H$, for $i = 1, 2, ..., R$, (5.24) can be written as follows,

$$d^2(\mathbf{x}, \hat{\mathbf{x}}) \approx \sum_{i=1}^{R} \gamma_i \sum_{l_{R_iD=0}}^{L_{R_iD}} \mathbf{h}_{R_iD}(l_{R_iD})^2 \mathbf{h}_{SR_i}^T \Re_i (\mathbf{h}_{SR_i}^T)^H. \tag{5.26}$$

Defining Θ_i =diag($\mathbf{v}_i$) and $\mu_{SR_i} = {\Theta_i}^{-1/2}\mathbf{h}_{SR_i}$, and $\mathbf{A}_{SR_i} = \Theta_i^{1/2}\Re_i\Theta_i^{1/2}$, we have

$$d^2(\mathbf{x}, \hat{\mathbf{x}}) \approx \sum_{i=1}^{R} \gamma_i \sum_{l_{R_iD=0}}^{L_{R_iD}} \mathbf{h}_{R_iD}(l_{R_iD})^2 \mu_{SR_i}^T \mathbf{A}_{SR_i} (\mu_{SR_i}^T)^H, \tag{5.27}$$

where $\mathbf{A}_{SR_i}$ are Hermitian and full rank. Therefore, there exists a unitary matrix $\mathbf{U}_{\mathbf{A}_{SR_i}}$ such that $\mathbf{U}^H_{\mathbf{A}_{SR_i}}\mathbf{A}_{SR_i}\mathbf{U}_{\mathbf{A}_{SR_i}} = \Delta_{SR_i}$, where Δ_{SR_i} is a diagonal matrix with elements equal to the eigenvalues of $\mathbf{A}_{SR_i}$. Therefore, (5.27) can be expressed as

$$d^2(\mathbf{x}, \hat{\mathbf{x}}) \approx \sum_{i=1}^{R} \gamma_i \sum_{l_{R_iD}=0}^{L_{R_iD}} \mathbf{h}_{R_iD}(l_{R_iD})^2 \beta_{SR_i} \Delta_{SR_i} \beta^H_{SR_i}, \tag{5.28}$$

where $\beta_{SR_i} = \mu^T_{SR_i}\mathbf{U}_{\mathbf{A}_{SR_i}}$. Thus, (5.28) can be simplified to

$$d^2(\mathbf{x}, \hat{\mathbf{x}}) \approx \sum_{i=1}^{R} \gamma_i \sum_{l_{R_iD}=0}^{L_{R_iD}} |\mathbf{h}_{R_iD}(l_{R_iD})|^2 \sum_{l_{SR_i=0}}^{L_{SR_i}} \lambda_{SR_i}(l_{SR_i})|\beta_{SR_i}(l_{SR_i})|^2, \tag{5.29}$$

where $\lambda_{SR_i}(l_{SR_i})$ denotes the $l^{th}_{SR_i}$ eigenvalue of codeword difference matrixes and β_{SR_i} is a zero-mean complex Gaussian vector with unit variance. Note that since both $S \rightarrow R_i$ and $R_i \rightarrow D$ links are frequency selective Rician fading, the PEP analysis for both cases $L_{R_iD} > L_{SR_i}$ and $L_{SR_i} > L_{R_iD}$ are similar. In the following, we derive the PEP expression for the case where $L_{R_iD} > L_{SR_i}$ and later extend it's results to the case where $L_{SR_i} > L_{R_iD}$.

Case I: $L_{R_iD} > L_{SR_i}$:

First, we define the random variable $Y = \prod_{i=1}^{R} Y_i = \prod_{i=1}^{R} X_{i1}X_{i2}$ with $X_{i1} = \sum_{lR_iD=0}^{L_{R_iD}} |\mathbf{h}_{R_iD}(l_{R_iD})|^2$ and $X_{i2} = \sum_{l_{SR_i}=0}^{L_{SR_i}} \lambda_{SR_i}(l_{SR_i})|\beta_{SR_i}(l_{SR_i})|^2$. Substituting (5.29) in (5.22) and averaging the resulting expression with respect to Y_1, Y_2, , Y_R, we obtain

$$\begin{aligned} P(\mathbf{x}, \hat{\mathbf{x}}) &\leq E_{Y_1}\left[\exp\left(-\tfrac{\gamma_1}{4N_0}Y_1\right)\right] ... E_{Y_R}\left[\exp\left(-\tfrac{\gamma_R}{4N_0}Y_R\right)\right] \\ &= \Phi_{Y_1}(\omega)|_{j\omega=-\frac{\gamma_1}{4N_0}} \times \Phi_{Y_2}(\omega)|_{j\omega=-\frac{\gamma_2}{4N_0}} \times ... \times \Phi_R(\omega)|_{j\omega=-\frac{\gamma_R}{4N_0}} \end{aligned}, \tag{5.30}$$

where $\Phi_{Y_1}(\omega)$, , and $\Phi_{Y_R}(\omega)$ are the characteristic functions of Y_1, , and Y_R respectively. $\Phi_{Y_i}(\omega)$ can be evaluated as [62]

$$\Phi_{Y_i}(\omega) = \int_0^{\infty} f_{X_{i1}}(x_{i1})\Phi_{X_{i2}}(\omega x_{i1})dx_{i1}, \tag{5.31}$$

where $f_{X_{i1}}(x_{i1})$, $x_1 \geq 0$ is the pdf of X_{i1}, and $\phi_{X_{i2}}(\omega x_{i1})$ is the characteristic function of

X_{i2}. Using the Rician pdf given in [61],

$$f_{X_{i1}}(x_{i1}) = \left(\frac{(L_{R_iD}+1+K_{R_iD})}{1/(L_{R_iD}+1)}\right) \times \left[\frac{(L_{R_iD}+1+K_{R_iD})}{K_{R_iD}\big(1/(L_{R_iD}+1)\big)}x_{i1}\right]^{L_{R_iD}/2} \times e^{-\left[K_{R_iD}+\frac{(L_{R_iD}+1+K_{R_iD})}{1/(L_{R_iD}+1)}x_{i1}\right]} \times I_{L_{R_iD}}\left[2\sqrt{\frac{K_{R_iD}(L_{R_iD}+1+K_{R_iD})}{1/(L_{R_iD}+1)}x_{i1}}\right], \tag{5.32}$$

where $K_{R_iD} = \sum_{l_{R_iD}=0}^{L_{R_iD}} K_{l_{R_iD}}$, and $K_{l_{R_iD}}$ is the Rician parameter on the ${l_{R_iD}}^{th}$ tap. Moreover, $\phi_{X_{i2}}(\omega x_{i1})$ can be evaluated as [61]

$$\phi_{X_{i2}}(wx_{i1}) = \prod_{l_{SR_i}=0}^{L_{SR_i}} \left[\frac{1+K_{l_{SR_i}}}{1+K_{l_{SR_i}} - w\lambda_{SR_i}(l_{SR_i})x_{i1}} e^{\frac{K_{l_{SR_i}} w\gamma_i x_{i1}}{1+K_{l_{SR_i}} - w\gamma_i x_{i1}}}\right]. \tag{5.33}$$

Using (5.33) and (5.32), (5.31) can be evaluated as

$$\begin{aligned}\phi_{Y_i}(\omega)\big|_{s=\frac{-\gamma_i}{4N_0}} &= (L_{R_iD}+1)(L_{R_iD}+1+K_{R_iD}) \times \int_0^\infty \left[\frac{(L_{R_iD}+1+K_{R_iD})}{K_{R_iD}\big(1/(L_{R_iD}+1)\big)}x_{i1}\right]^{L_{R_iD}/2} \\ &\times e^{-\left[K_{R_iD}+\frac{(L_{R_iD}+1+K_{R_iD})}{1/(L_{R_iD}+1)}x_{i1}\right]} \times I_{L_{R_iD}}\left[2\sqrt{K_{R_iD}(L_{R_iD}+1+K_{R_iD})(L_{R_iD}+1)x_{i1}}\right] \\ &\times \prod_{l_{SR_i}=0}^{L_{SR_i}} \left[\frac{1+K_{l_{SR_i}}}{1+K_{l_{SR_i}} - w\lambda_{SR_i}(l_{SR_i})x_{i1}} e^{\frac{K_{l_{SR_i}} w\gamma_i x_{i1}}{1+K_{l_{SR_i}} - w\gamma_i x_{i1}}}\right] dx_{i1}.\end{aligned} \tag{5.34}$$

Introducing $c = (L_{R_iD}+1)(L_{R_iD}+1+K_{R_iD})$ and $I_{L_{R_iD}}(\alpha) = \left(\frac{\alpha}{2}\right)^{L_{SR}} \sum_{k=0}^{\infty} \left(\frac{\alpha^2}{4}\right)^k \frac{1}{k!\Gamma(k+L_{R_iD}+1)}$, and assuming high SNR values and perfect power control, i.e., $E_{R_1D} = E_{R_2D} = ... = E_{R_RD}$ and large enough SNR values in the $S \to R_i$ links, i.e., $\frac{E_{SR_i}}{N_0} \gg 1$, $\gamma_1 = \gamma_2 = ... = \gamma_R = E_R$, (5.34) can be further simplified to

$$\begin{aligned}\phi_{Y_i}(\omega)\big|_{s=\frac{-E_R}{4N_0}} &= c\left(\frac{c}{K_{R_iD}}\right)^{L_{R_iD}/2} e^{-K_{R_iD}} \times \int_0^\infty x_{i1}^{L_{R_iD}/2} e^{-cx_{i1}} \left(\sqrt{K_{R_iD}cx_{i1}}\right)^{L_{R_iD}} \\ &\times \sum_{k=0}^{\infty} (K_{R_iD}cx_{i1})^k \frac{1}{k!\Gamma(k+L_{R_iD}+1)} \times \prod_{l_{SR_i}=0}^{L_{SR_i}} \left[\frac{1+K_{l_{SR_i}}}{1+K_{l_{SR_i}} - w\lambda_{SR_i}(l_{SR_i})x_{i1}} e^{\frac{K_{l_{SR_i}} wE_R x_{i1}}{1+K_{l_{SR_i}} - wE_R x_{i1}}}\right] dx_{i1}.\end{aligned} \tag{5.35}$$

Assuming high SNR in $S \rightarrow R_i$, $i = 1, 2, ..., R$, i.e., $E_{SR_i}/N_0 \gg 1$, (5.35) yields

$$\begin{aligned}\phi_{Y_i}(\omega)|_{s=\frac{-E_R}{4N_0}} &= e^{-K_{SR_i}} \left(\prod_{l_{SR_i}=0}^{L_{SR_i}} 1 + K_{l_{SR_i}}\right) s^{-(L_{SR_i}+1)} \times (\lambda_{SR_i})^{-(L_{SR_i}+1)} c \times \left(\frac{c}{K_{R_iD}}\right)^{L_{R_iD}/2} \\ &\times e^{-K_{R_iD}} \int_0^\infty x_{i1}^{L_{R_iD}/2} e^{-cx_{i1}} \left(\sqrt{K_{R_iD} c x_{i1}}\right)^{L_{R_iD}} \times \sum_{k=0}^{\infty} (K_{R_iD} c x_{i1})^k \frac{1}{k!\Gamma(k+L_{R_iD}+1)} x_{i1}^{L_{SR_i}-1} dx_{i1}.\end{aligned} \tag{5.36}$$

After further mathematical manipulation, (5.36) can be expressed as

$$\begin{aligned}\phi_{Y_i}(\omega)|_{s=\frac{-E_R}{4N_0}} &= e^{-K_{SR_i}-K_{R_iD}} \prod_{l_{SR_i}=0}^{L_{SR_i}} \left(1 + K_{l_{SR_i}}\right) c^{L_{SR_i}-L_{R_iD}/2+1} s^{-(L_{SR_i}+1)} (\lambda_{SR_i})^{-(L_{SR_i}+1)} \\ &\times \sum_{k=0}^{\infty} \frac{\left(K_{R_iD}\right)^k \Gamma(-L_{SR_i}+L_{R_iD}+k)}{k!\Gamma(k+L_{R_iD}+1)}.\end{aligned} \tag{5.37}$$

Substituting (5.37) in (5.30), we find the final PEP expression given as

$$\begin{aligned}P(\mathbf{x}, \hat{\mathbf{x}}) &\leq \prod_{i=1}^{R} e^{-K_{SR_i}-K_{R_iD}} \prod_{l_{SR_i}=0}^{L_{SR_i}} \left(1 + K_{l_{SR_i}}\right) (L_{R_iD}+1)^{L_{SR_i}-L_{R_iD}/2+1} \\ &\times (L_{R_iD}+1+K_{R_iD})^{L_{SR_i}-L_{R_iD}/2+1} \times \left(\frac{E_R}{4N_0}\right)^{-(L_{SR_i}+1)} (\lambda_{SR_i})^{-(L_{SR_i}+1)} \\ &\times \sum_{k=0}^{\infty} \frac{\left(K_{R_iD}\right)^k \Gamma(-L_{SR_i}+L_{R_iD}+k)}{k!\Gamma(k+L_{R_iD}+1)}.\end{aligned} \tag{5.38}$$

It is observed from (5.38) that the maximum achievable diversity order is given by $\sum_{i=1}^{R} L_{SR_i} + R$.

Case II: $L_{SR_i} > L_{R_iD}$:

By interchanging L_{SR_i} and L_{R_iD} and noting that this case is similar to case I, we can write the PEP as

$$\begin{aligned}P(\mathbf{x}, \hat{\mathbf{x}}) &\leq \prod_{i=1}^{R} e^{-K_{SR_i}-K_{R_iD}} \prod_{l_{R_iD}=0}^{L_{R_iD}} \left(1 + K_{l_{R_iD}}\right) (L_{SR_i}+1)^{L_{R_iD}-L_{SR_i}/2+1} \\ &\times (L_{SR_i}+1+K_{SR_i})^{L_{R_iD}-L_{SR_i}/2+1} \left(\frac{E_R}{4N_0}\right)^{-(L_{R_iD}+1)} (\lambda_{R_iD})^{-(L_{R_iD}+1)} \\ &\times \sum_{k=0}^{\infty} \frac{\left(K_{SR_i}\right)^k \Gamma(-L_{R_iD}+L_{SR_i}+k)}{k!\Gamma(k+L_{SR_i}+1)}.\end{aligned} \tag{5.39}$$

It is observed from (5.39) that the maximum achievable diversity order is given by $\sum_{i=1}^{R} L_{R_iD} + R$. Based on (5.38) and (5.39), we conclude that the maximum achievable diversity order for the general case is given by $\sum_{i=1}^{R} \min(L_{SR_i}, L_{R_iD}) + R$. This is consistent with the results

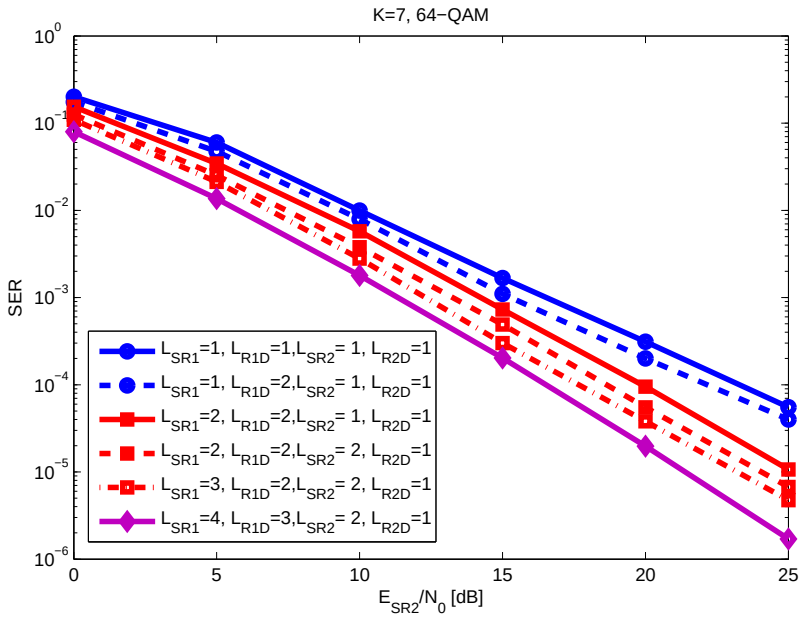

Figure 5.1: SER performance of the DSTBC SC-FDE system with two relays.

reported in [3] for a single relay scenario over Rayleigh fading channels. Through the two above cases, we can conclude that the value of n in the Rician fading channels, causes the reduction of PEP and doesn't affect the diversity gain.

5.5 Numerical Results

In this section, we present Monte-Carlo simulation results for the proposed receiver assuming a quasi-static frequency-selective Rician fading channels, which are suitable for suburban areas that a LOS path often exists. Rician fading is characterized by the K factor ($K = n^2$), which is the power ratio of the LOS and the diffused components. It represents Rayleigh fading for $K = 0$, and no fading when $K \to \infty$. The channel impulse responses CIRs are modeled as frequency-selective Rician fading channels and a uniform delay power profile. Furthermore, with the assumption that $\frac{E_{SR_2}}{N_0} = \frac{E_{R_iD}}{N_0} \gg 1$, $i = 1, ..., R$, and $\frac{E_{SR_i}}{N_0} \gg \frac{E_{SR_2}}{N_0}$, $i = 1, ..., R$, $i \neq 2$, the scaling coefficients γ_i in (5.6) can be approximated as $\gamma_1 = ... = \gamma_R = E_{SR_2}$.

First, we assume that there are two relay nodes, where each node is equipped with one antenna. We set $\text{SNR}_{SR_1} = 25\text{dB}$ and $\text{E}_{R_1D} = \text{E}_{R_2D} = 5\text{dB}$, and the SER curve is plotted

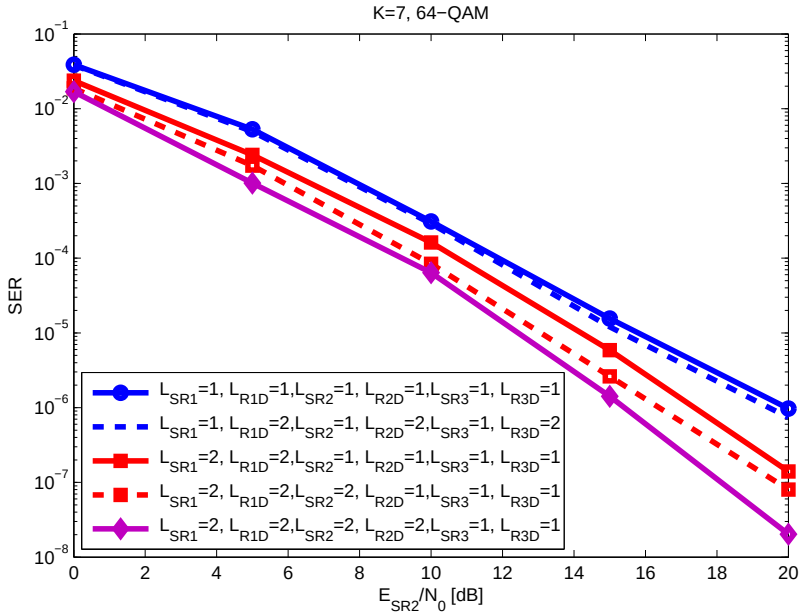

Figure 5.2: SER performance of the DSTBC SC-FDE system with three relays.

against $\frac{E_{SR_2}}{N_0}$. 64-QAM modulation and $\mathcal{G}_2$ code [20] are used. Additionally, we assume that $K = 7$ for all links. The scenarios with different combinations of channel memory lengths are considered:

1) $L_{SR_1} = 1, L_{R_1D} = 1, L_{SR_2} = 1, L_{R_2D} = 1,$

2) $L_{SR_1} = 1, L_{R_1D} = 2, L_{SR_2} = 1, L_{R_2D} = 1,$

3) $L_{SR_1} = 2, L_{R_1D} = 2, L_{SR_2} = 1, L_{R_2D} = 1,$

4) $L_{SR_1} = 2, L_{R_1D} = 2, L_{SR_2} = 2, L_{R_2D} = 1,$

5) $L_{SR_1} = 3, L_{R_1D} = 2, L_{SR_2} = 2, L_{R_2D} = 1,$

6) $L_{SR_1} = 4, L_{R_1D} = 3, L_{SR_2} = 2, L_{R_2D} = 1.$

As can be noticed from Fig. 5.1, the SER curves in the first two, next three, and the last two scenarios have identical slopes for high $\frac{E_{SR_2}}{N_0}$ values, achieving the full diversity order of $\sum_{i=1}^{2} \min(L_{SR_i}, L_{R_iD}) + 2$, as predicted.

Secondly, we assume that there are three relay nodes, where each node is equipped with

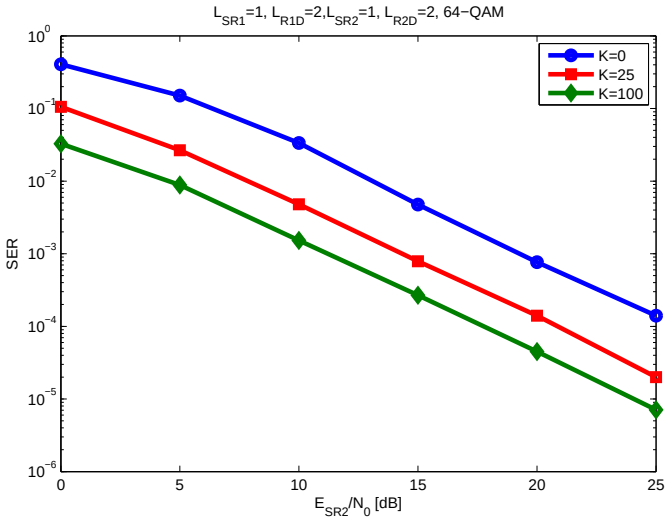

Figure 5.3: SER performance of the DSTBC SC-FDE system for different K-factor values.

one antenna. We set $\text{SNR}_{SR_1} = \text{SNR}_{SR_3} = 25\text{dB}$ and $\text{E}_{R_1D} = \text{E}_{R_2D} = \text{E}_{R_3D} = 5\text{dB}$, and the SER curve is plotted against $\frac{E_{SR_2}}{N_0}$. 64-QAM modulation and $\mathcal{G}_3$ code [20] are used. Additionally, we assume that $K = 7$ for all links. The scenarios with different combinations of channel memory lengths are considered:

1) $L_{SR_1} = L_{R_1D} = L_{SR_2} = L_{R_2D} = L_{SR_3} = L_{R_3D} = 1$,

2) $L_{SR_1} = L_{SR_2} = L_{SR_3} = 1, L_{R_1D} = L_{R_2D} = L_{R_3D} = 2$,

3) $L_{SR_1} = L_{R_1D} = 2, L_{SR_2} = L_{R_2D} = L_{SR_3} = L_{R_3D} = 1$,

4) $L_{SR_1} = L_{R_1D} = L_{SR_2} = 2, L_{R_2D} = L_{SR_3} = L_{R_3D} = 1$,

5) $L_{SR_1} = L_{R_1D} = L_{SR_2} = L_{R_2D} = 2, L_{SR_3} = L_{R_3D} = 1$,

As is illustrated in Fig. 5.2, first two and their next two scenarios have identical slopes for high $\frac{E_{SR_2}}{N_0}$ values, achieving the full diversity order of $\sum_{i=1}^{3} \min(L_{SR_i}, L_{R_iD}) + 3$, confirming our conclusions from the PEP analysis.

Finally, the SER performance of the system is illustrated in Fig. 5.3 for different K-factor values. We set $\text{SNR}_{SR_1} = 25\text{dB}$ and $\text{E}_{R_1D} = \text{E}_{R_2D} = 5\text{dB}$, and the SER curve is plotted against $\frac{E_{SR_2}}{N_0}$. 64-QAM modulation and $\mathcal{G}_2$ code [20] are used. Additionally, we assume that $L_{SR_1} = L_{SR_2} = 1$ and $L_{R_1D} = L_{R_2D} = 2$ and plot the SER curves when

$K = 0$, $K = 25$, and $K = 100$ for all of the underlying links. We remark that as the K-factor of the Rician fading increases, the better SER performance is achieved, while the diversity order remains unchanged.

As can be concluded from the simulation results that, in dual hop networks, the hop with the smaller diversity order becomes the performance bottleneck.

5.6 Summary

In this chapter, by characterizing the channels as frequency-selective Rician fading, we have derived theoretical PEP expression for distributed space-time block code in AF relaying mode. Various numerical examples have been introduced to confirm our theoretical analysis. Furthermore, we have investigated the performance of the distributed space-time block code under different fading severity conditions.

Chapter 6

Conclusion

6.1 Conclusions

In this thesis, we investigate efficient equalization techniques for broadband wireless networks. These low-complexity and efficient equalization techniques address non-cooperative and cooperative wireless networks.

We first study a new detection scheme for ZP-OFDM. We propose a novel reduced complexity receiver design for ZP-OFDM transmissions, that not only outperforms MMSE-ZP-OFDM, but also uses low-complexity computational methods that bring a significant power saving to the proposed receiver. This makes it a strong candidate for WSNs which are characterized by small and low-power devices. We show that linear processing collects both multipath and spatial diversity gains, leading to significant improvement in performance, while maintaining low complexity.

We next introduce a novel MMSE-based receiver design for SC-FDE. We propose a novel reduced-complexity MMSE-based receiver design for D-STBC SC-FDE transmissions. Specifically, we are considering AF relay networks for cooperative scenarios in which either of $S \rightarrow R$ or $R \rightarrow D$ links are frequency selective Rician fading. We show that, by incorporating linear processing techniques, our MMSE-based receiver is able to collect full antenna and multipath diversity gains, leading to significant improvement in performance at nearly no additional complexity. Specifically, under the assumption of perfect power control and high SNR for the underlying links and assuming either of $S \rightarrow R$ or $R \rightarrow D$ links to be frequency selective Rician fading, our performance analysis demonstrates that the proposed receiver is able to achieve a maximum diversity order of $\min(L_{SR}, L_{RD}) + L_{SD} + 2$, where

L_{SR}, L_{RD}, and L_{SD} are the channel memory lengths for $S \rightarrow R$, $R \rightarrow D$, and $S \rightarrow D$ links, respectively. Complexity analysis and simulation results demonstrate that our proposed receiver outperforms the conventional cooperative MMSE-SC-FDE receiver by performing close to MFB, while providing minimal computational complexity.

Finally, we investigate the performance of D-STBC SC-FDE systems with AF relaying over frequency-selective Rician fading channels in multi-relay networks. Our performance analysis demonstrates that SC-FDE for DSTBC is able to achieve a maximum diversity order of $\sum_{i=1}^{R} \min(L_{SR_i}, L_{R_iD}) + R$, where R is the number of participating relays, L_{SR_i} and L_{R_iD} are the channel memory lengths for source to i^{th} relay ($S \rightarrow R_i$) link and i^{th} relay to destination ($R_i \rightarrow D$) link , respectively.

6.2 Future works

The works in this thesis also reveal some interesting topics for future research. A particularly intriguing problem is to analyze the efficiency of the low-complexity ZP-OFDM receiver design described in chapter 3, as well as the efficient MMSE-based D-STBC SC-FDE receiver described in chapter 4, in presence of multiple users.

In the study of DSTBC SC-FDE for multi-relay networks, we have mainly focused on the application of different STBCs. This, however, brings about throughput loss and lower efficiency. An interesting future work on this subject is to investigate a relay selective algorithm for frequency selective channels that makes up for the STBC rate loss.

Bibliography

[1] B. Muquet, Z. Wang, G. B. Giannakis, M. de Courville, and P. Duhamel, "Cyclic prefixing or zero padding for wireless multicarrier transmissions?" *IEEE Trans. Commun*, vol. 50, pp. 2136–2148, 2002.

[2] H. Eghbali, S. Muhaidat, and N. Al-Dhahir, "A novel reduced complexity mmse-based receiver for ofdm broadband wireless networks," in *IEEE Wireless Comm. and Networking Conf. (WCNC)*, Sydney, Aus, 2010.

[3] H. Mheidat, M. Uysal, and N. Al-Dhahir, "Equalization techniques for distributed space-time block codes with amplify-and-forward relaying," *IEEE Trans. on Signal Proc*, vol. 55, no. 5, 2007.

[4] D. Y. Seol, U. K. Kwon, and E. S. Kim, "Relay-assisted sfbc single carrier transmission over uplink fast fading channels," in *Proc. IEEE GLOBECOM*, 2007.

[5] H. Eghbali, S. Muhaidat, and N. Al-Dhahir, "A low complexity two stage mmse-based receiver for single-carrier frequency-domain equalization transmissions over frequency-selective channels," in *Proc. IEEE GLOBECOM*, Honolulu, Hawaii, USA, 2009.

[6] S. Y. Hui and K. H. Yeung, "Challenges in the migration to 4g mobile systems," *IEEE Commun. Mag.*, vol. 41, pp. 54 – 59, 2003.

[7] T. S. Rappaport, *Wireless Communications: Principles and Practice*, 2nd ed. Upper Saddle River, NJ: Prentice-Hall, 2002.

[8] W. C. Jakes, *Microwave Mobile Communications*, 1st ed. New York: John Wiley and Sons, 1974.

[9] D. Tse and P. Viswanath, *Fundamentals of Wireless Communication*. Cambridge University Press, 2005.

[10] S. M. Alamouti, "A simple transmit diversity technique for wireless communications," *IEEE J. Sel. Areas Commun.*, vol. 16, pp. 1451–1458, 1998.

[11] J. Rogers and C. Plett, *Radio frequency integrated circuit design*, 2nd ed. London, United Kingdom: Artech House, 2010.

[12] A. Wittneben, "Base station modulation diversity for digital simulcast," in *Proc. of Vehicular Technology Conference. VTC-93.*, 1993, pp. 505–511.

[13] ——, "A new bandwidth efficient transmit antenna modulation diversity scheme for linear digital modulation," in *Proceedings of the IEEE International Conference Communications (ICC)*, 1993, pp. 1630–1634.

[14] J. H. Winters, "Diversity gain of transmit diversity in wireless systems with rayleigh fading," *IEEE Trans. Veh. Technol.*, vol. 47, pp. 119–123, 1998.

[15] V. Tarokh, N. Seshadri, and A. R. Calderbank, "Space-time codes for high data rate wireless communication: Performance criterion and code construction," *IEEE Trans. Inf. Theory*, vol. 44, pp. 744–765, 1998.

[16] J. G. Foschini, "Layered space-time architecture for wireless communication in a fading environment when using multi element antennas," *Bell Labs Tech. J.*, vol. 2, pp. 41–59, 1996.

[17] C. Kose and R. D. Wesel, "Universal space-time trellis codes," *IEEE Trans. Inf. Theory*, vol. 49, pp. 2717–2727, 2003.

[18] Z. Safar and K. J. R. Liu, "Systematic space-time trellis code construction for correlated rayleigh-fading channels," *IEEE Trans. Inf. Theory*, vol. 50, pp. 2855–2865, 2004.

[19] L. Yonghui, B. Vucetic, Y. Tang, and Q. Zhang, "Space-time trellis codes with li-near transformation for fast fading channels," *IEEE Signal Process. Lett.*, vol. 50, no. 11, pp. 895– 898, 2004.

[20] V. Tarokh, H. Jafarkhani, and A. R. Calderbank, "Space-time block codes from orthogonal designs," *IEEE Trans. Inf. Theory*, vol. 45, pp. 1456–1467, 1999.

[21] V. Tarokh, A. Naguib, N. Seshadri, and A. R. Calderbank, "Spacetime codes for wireless communication: Combined array processing and space time coding," *IEEE Trans. Inf. Theory*, vol. 45, 1998.

[22] H. Wang and X.-G. Xia, "Upper bounds of rates of complex orthogonal space-time block codes," *IEEE Trans. Inf. Theory*, vol. 49, no. 10, pp. 2788–2796, 2003.

[23] S. Das, N. Al-Dhahir, and R. Calderbank, "Novel full-diversity high-rate stbc for 2 and 4 transmit antennas," *IEEE Commun. Lett.*, vol. 10, no. 3, pp. 171–173, 2006.

[24] H. Jafarkhani and N. Seshadri, "Super-orthogonal space-time trellis codes," *IEEE Trans. Inf. Theory*, vol. 49, no. 4, pp. 937–950, 2003.

[25] B. Hassibi and B. Hochwald, "High-rate codes that are linear in space and time," *IEEE Trans. Inf. Theory*, vol. 48, no. 7, pp. 1804–1824, 2002.

[26] R. W. Heath and A. Paulraj, "Linear dispersion codes for mimo systems based on frame theory," *IEEE Trans. Signal Process.*, vol. 50, no. 10, pp. 2429–2441, 2002.

[27] B. Vucetic and J. Yuan, *Space-Time Coding.* John Wiley & Sons, 2003.

[28] A. Paulraj, D. Gore, and R. Nabar, *Introduction to Space-Time Wireless Communications.* Cambridge University Press, 2003.

[29] H. Jafarkhani, *Space-Time Coding: Theory and Practice.* Cambridge University Press, 2005.

[30] A. Sendonaris, E. Erkip, and B. Aazhang, "User cooperation diversity part i: system description," *IEEE Trans. Comm.*, vol. 51, no. 11, 2003.

[31] ——, "User cooperation diversity part ii: implementation aspects and performance analysis," *IEEE Trans. Comm.*, vol. 51, no. 11, 2003.

[32] J. N. Laneman, G. W. Wornell, and D. N. C. Tse, "An efficient protocol for realizing cooperative diversity in wireless networks," Washington, DC.

[33] J. N. Laneman, D. N. C. Tse, and G. W. Wornell, "Cooperative diversity in wireless networks: Efficient protocols and outage behavior," *IEEE Trans. Inf. Theory*, 2004.

[34] J. N. Laneman and G. W. Wornell, "Distributed space-time-coded protocols for exploiting cooperative diversity in wireless networks," *IEEE Trans. Inf. Theory*, vol. 49, no. 10, 2003.

[35] E. V. D. Meulen, "Advances in applied probability," *Advances in Applied Probability*, vol. 3, pp. 120–154, 1971.

[36] T. M. Cover and A. E. Gamal, "Capacity theorems for the relay channel," *IEEE Trans. Inf. Theory*, vol. 25, no. 5, 1979.

[37] T. E. Hunter and A. Nosratinia, "Cooperative diversity through coding," in *Proc. IEEE ISIT*, Lausanne, Switzerland, 2002.

[38] ——, "Diversity through coded cooperation," *IEEE Trans. Wireless Commun.*, vol. 5, no. 2, pp. 283–289, 2006.

[39] R. U. Nabar, H. Bolcskei, and F. Kneubuhler, "Fading relay channels: Performance limits and space-time signal design," *IEEE J. Sel. Areas Comm.*, vol. 22, no. 6.

[40] A. Azarian, H. EL Gamal, and P. Schniter, "On the achievable diversity multiplexing tradeoff in half-duplex cooperative channels," *IEEE Trans. Inf. Theory*, vol. 51, pp. 4152–4172, 2005.

[41] J. E. Padgett, C. G. Gunther, and T. Hattori, "Overview of wireless personal communications," *IEEE Commun. Mag.*, vol. 33, no. 1, pp. 28–41, 1995.

[42] J. D. Parsons, *The Mobile Radio Propagation Channel*, 2nd ed. Singapore: John Wiley & Sons, 2000.

[43] A. Goldsmith, *Wireless Communications*, 1st ed. UK: Cambridge University Press, 2005.

[44] D. Falconer and et. al., "Frequency domain equalization for single-carrier broadband wireless systems," *IEEE Commun. Mag.*, vol. 40, no. 4, pp. 58–66, 2002.

[45] H. Sari, G. Karam, and I. Jeanclaude, "Frequency-domain equalization of mobile radio and terrestrial broadcast channels," in *Proc. of Global Telecommunications Conference. GLOBECOM-94*, 1994, p. 15.

[46] Z. Wang and G. B. Giannakis, "Linearly precoded or coded ofdm against wireless channel fades?" in *Proc. of the IEEE Workshop on Signal Processing Advances for Wireless Communications*, Taiwan, China, 2001.

[47] W. W. Lu, "Compact multidimensional broadband wireless: The convergence of wireless mobile and access," *IEEE Commun. Mag.*, pp. 119–23, 2000.

[48] S. Govardhanagiri, T. Karp, P. Heller, and T. Nguyen, "Performance analysis of multicarrier modulations systems using cosine modulated filterbanks," in *Proc. ICASSP*.

[49] D. P. Palomar, J. M. Cioffi, and M. A. Lagunas, "Joint tx-rx beamforming design for multicarrier mimo channels: a unified framework for convex optimization," *IEEE Trans. Signal Process*, vol. 51, no. 9, 2003.

[50] W. Zou and Y. Wu, "Cofdm : an overview," *IEEE Trans. Broadcast*, vol. 41, 1995.

[51] D. Divsalar and M. K. Simon, "Multiple trellis coded modulation (mtcm)," *IEEE Trans. Commun*, vol. 36, 1988.

[52] ——, "Error bounds for convolutional codes and an asymptotically optimum decoding algorithm," *IEEE Trans. Inform. Theory*, vol. IT-13, 1967.

[53] L. Lee, "Space-time bit-interleaved coded modulation for ofdm systems," *IEEE Trans. Signal Process*, vol. 52, 2004.

[54] Z. Liu, Y. Xin, and G. B. Giannakis, "Linear constellation precoding for ofdm with maximum multipath diversity and coding gains," *IEEE Trans. Commun*, vol. 51, 2003.

[55] J. Boutros and E. Viterbo, "Signal space diversity: a power- and bandwidth-efficient diversity technique for the rayleigh fading channel," *IEEE Trans. Inform. Theory*, vol. 44, 1998.

[56] A. O. Hero and T. L. Marzetta, "Cutoff rate and signal design for the quasi-static rayleigh fading space-time channel," *IEEE Trans. Inform. Theory*, vol. 47, 2001.

[57] Y. Rong, S. A. Vorobyov, and A. B. Gershman, "Linear block precoding for ofdmsystems based on maximization of mean cutoff rate," *IEEE Trans. Signal Process*, vol. 53, no. 12, 2005.

[58] O. Edfors, M. Sandell, J. J. van de Beek, and P. O. Brjesson, "Ofdm channel estimation by singular value decomposition," *IEEE Comm. Lett.*, vol. 46, no. 7, pp. 931–939, 1998.

[59] J. Coon, S. Armour, M. Beach, and J. McGeehan, "Adaptive frequency-domain equalization for single-carrier multiple-input multiple-output wireless transmissions," *IEEE Trans. on Signal Proc*, vol. 53, no. 8, pp. 3247–3256, 2005.

[60] A. Scaglione, G. B. Giannakis, and S. Barbarossa, "Redundant filterbank precoders and equalizers - part i : Unification and optimal designs and part ii : Blind channel estimation, synchronization and direct equalization," *IEEE Trans. Signal Process*, vol. 47, 1999.

[61] M. K. Simon and M. S. Alouini, *Digital Communication Over Fading Channels: A Unified Approach to Performance Analysis*. New York: Wiley-Intersci., 2000.

[62] A. Stuart and J. K. Ord, *Kendall's Advanced Theory of Statistics*, 5th ed. London, U.K.: Griffin, 1987.

[63] J. Lu, T. T. Tjhung, F. Adachi, and C. L. Huang, "Ber performance of ofdm-mdpsk system in frequency-selective rician fading with diversity reception," *IEEE Trans. on Veh. Technol.*, vol. 49, no. 4, pp. 1216–1225, 2000.

[64] N. Al-Dhahir, "Single-carrier frequency-domain equalization for spacetime block-coded transmissions over frequency-selective fading channels," *Electron. Lett.*, vol. 5, pp. 304–306, 2001.

[65] M. Uysal, O. Campolat, and M. M. Fareed, "Asymptotic performance analysis of distributed space-time codes," *IEEE Commun. Lett.*, vol. 10, no. 11, pp. 775–777, 2006.

[66] O. Canpolat, M. Uysal, and M. M. Fareed, "Analysis and design of distributed space-time trellis codes with amplify-and-forward relaying," *IEEE Trans. Veh. Technol.*, vol. 56, pp. 1649–1660, 2007.

[67] R. U. Nabar1 and H. Bolcskei, "Space-time signal design for fading relay channels," in *Proc. IEEE GLOBECOM*, vol. 4, San Francisco, CA., 2003.